HHS Public Access

Author manuscript

Glia. Author manuscript; available in PMC 2017 November 09.

Published in final edited form as:

Glia. 2012 October ; 60(10): 1451–1467. doi:10.1002/glia.22365.

Laminin regulates postnatal oligodendrocyte production by promoting oligodendrocyte progenitor survival in the subventricular zone

Jenne Relucio[1], **Michael J. Menezes**[1], **Yuko Miyagoe-Suzuki**[2], **Shin'ichi Takeda**[2], and **Holly Colognato**[1,*]

[1]Department of Pharmacology, Stony Brook University, Stony Brook, NY 11794 USA

[2]Department of Molecular Therapy, National Center of Neurology and Psychiatry, Ogawa-higashi, Kodaira, Tokyo 187-8502 Japan

Abstract

The laminin family of extracellular matrix proteins are expressed broadly during embryonic brain development, but are enriched at ventricular and pial surfaces where laminins mediate radial glial attachment during corticogenesis. In the adult brain, however, laminin distribution is restricted, yet is found within the vascular basal lamina and associated fractones of the ventricular zone (VZ)-subventricular zone (SVZ) stem cell niche, where laminins regulate adult neural progenitor cell proliferation. It remains unknown, however, if laminins regulate the wave of oligodendrogenesis that occurs in the neonatal/early postnatal VZ-SVZ. Here we report that *Lama2*, the gene that encodes the laminin α2-subunit, regulates postnatal oligodendrogenesis. At birth, *Lama2*−/− mice had significantly higher levels of dying oligodendrocyte progenitor cells (OPCs) in the OPC germinal zone of the dorsal SVZ. This translated into fewer OPCs, both in the dorsal SVZ well as in an adjacent developing white matter tract, the corpus callosum. In addition, intermediate progenitor cells that give rise to OPCs in the *Lama2*−/− VZ-SVZ were mislocalized and proliferated nearer to the ventricle surface. Later, delays in oligodendrocyte maturation (with accompanying OPC accumulation), were observed in the *Lama2*−/− corpus callosum, leading to dysmyelination by postnatal day 21. Together these data suggest that pro-survival laminin interactions in the developing postnatal VZ-SVZ germinal zone regulate the ability, or timing, of oligodendrocyte production to occur appropriately.

Keywords

laminin; oligodendrocyte progenitor cell; gliogenesis; subventricular zone; survival

Introduction

In the developing CNS, neural stem cells (NSCs) and their progeny are influenced by the microenvironment of their germinal niches. For example, extrinsic signals such as extracellular matrix proteins regulate neurogenesis in the embryonic ventricular zone (VZ),

*Corresponding author: cologna to@pharm.stonybrook.edu, phone: 1-631-444-7815.

which serves as the primary site of embryonic NSC expansion and neurogenesis (Kang et al., 2009; Machon et al., 2003; Yu et al., 2007). During late neurogenesis a second pool of progenitors expands to form the ventricular zone (VZ) - subventricular zone (SVZ) germinal niche, which, by birth, has transitioned to being primarily gliogenic (Levison et al., 1993; Lewis and Lai, 1974; Marshall et al., 2005; Zerlin et al., 1995). By adulthood, the various cell types of the VZ-SVZ are organized in a complex arrangement in which extracellular matrix proteins and adhesion proteins contribute to the precise spatial organization needed to maintain a functional adult neural stem cell niche (Kazanis et al., 2010; Mirzadeh et al., 2008; Shen et al., 2008; Tavazoie et al., 2008). In contrast, while stem/progenitor cells of the early postnatal VZ-SVZ generate the wave of gliogenesis that occurs during the first few weeks of postnatal life, it remains unclear whether “niche architecture” contributes to the ability of the early postnatal VZ-SVZ to generate glia, and whether this architecture is influenced by adhesion and/or extracellular matrix interactions.

A role for the extracellular matrix protein laminin in postnatal myelination, however, was revealed by examination of the laminin α2-deficient *dy/dy* mouse, in which defects in oligodendrocyte maturation and myelination were observed (Chun et al., 2003; Relucio et al., 2009). The *dy/dy* mouse may model the human disease MDC1A, arising from mutations in *lama2*, the gene that encodes the laminin α2-subunit; MDC1A is a form of congenital muscular dystrophy that is accompanied by brain abnormalities such as agryrias and hypoplasias, in conjunction with cognitive deficits and seizures (Allamand and Guicheney, 2002; Buteică et al., 2008; Fujii et al., 2011; Miyagoe-Suzuki et al., 2000). The myelination defects in *dy/dy* mice were postulated to arise through dysregulation of local laminin-oligodendrocyte interactions in the developing white matter, not through defects in oligodendrogenesis. However, several studies have revealed that laminins regulate embryonic cortical *neurogenesis* (Halfter et al., 2002; Lathia et al., 2007; Loulier et al., 2009). In addition, α2-subunit-containing laminins are found in VZ-SVZ proliferative zones during embryonic development (Lathia et al., 2007), where they regulate cell attachment and organization (Loulier et al., 2009). Adhesion receptors, such as integrins that contain the β1 subunit, are expressed on the surface of NSCs and neural progenitors in germinal niches both during embryogenesis and in the adult, suggesting possible requirements for laminin-integrin interactions in regulating NSCs and/or their immediate progeny (Lathia et al., 2007). Together, these studies suggest that laminins may regulate the ordered genesis of neural cells in the developing brain, although the role of laminins in regulating gliogenesis has remained, to date, unknown.

In this study, we used laminin α2 null mice (LAMA2−/−) to determine whether α2-containing laminins regulate VZ-SVZ oligodendrogenesis in the neonatal/postnatal brain. We report that laminins, including α2, are present within the VZ-SVZ perinatally i.e. at the onset of postnatal oligodendrogenesis. Perinatal LAMA2−/− mice, however, had fewer oligodendrocyte progenitor cells (OPCs), both in the germinal VZ-SVZ and in an adjacent developing white matter tract, the corpus callosum. The cellular organization in the VZ-SVZ germinal niche was furthermore disturbed in laminin mutants, with proliferating intermediate progenitor cells found abnormally close to the ventricle surface. In conjunction, newly-born OPCs in the laminin-deficient SVZ showed substantially elevated levels of cell death. Oligodendrocyte maturation was subsequently defective in LAMA2−/− mice relative

to that of wildtype littermates, such that by 3-weeks of age, fewer mature oligodendrocytes were found in the corpus callosum, along with more OPCs and thinner myelin. Together our findings suggest that α2-containing laminins of the SVZ regulate cortical oligodendrogenesis, and, furthermore, that dysregulation of the gliogenic niche may contribute to CNS abnormalities observed in MDC1A.

Materials and Methods

Animals

Laminin α2 chain-null mice (LAMA2−/−) were described previously (Miyagoe et al., 1997). Heterozygous *lama2*+/− mice were bred to obtain homozygous mutants. Genotyping was performed on tail DNA to detect the *lama2* wildtype (WT) and mutant allele (Iwao et al., 2000). The primers used to detect the WT allele were: 5′–CCAGATTGCCTACGTAATTG–3′ and 5′–CCTCTCCATTTTCTAAAG–3′. PCR was performed using the primer pair 5′–CTTTCAGATTGCATTGCAAGC–3′ and 5′–TCGTTTGTTCGGATCCGTCG–3′ to detect the KO allele. Homozygous wildtype (+/+) and heterozygous littermates were used as age-matched controls. All procedures were performed in accordance with the NIH Guide for the Care and Use of Laboratory Animals and approved by the Stony Brook University IACUC.

Antibodies

The following rabbit polyclonal IgG antibodies were used: laminin-1 (Sigma); NG2 (Chemicon); PDGFRα (SantaCruz); Sox2 (Millipore); Pax6 (Millipore); GFAP (Dako); Olig2 (Immuno-Biological Laboratories). The following monoclonal IgG antibodies were used: laminin α2-subunit (rat, clone 4H82, Sigma); laminin gamma1 subunit (rat, clone A5, Millipore); nestin (mouse, BD-Pharmingen); CD140a i.e. PDGFRα (rat, BD-Pharmingen); myelin basic protein (rat, Serotec); PCNA (mouse, Cell Signaling); APC (mouse, CC1, Calbiochem); neurofilament200 (mouse, Sigma); β-actin (mouse, Sigma).

Laminin alpha2 fluorescent immunocytochemistry using frozen sections

Cerebral cortices collected from age-matched *lama2−/−* and control littermates were frozen, embedded in Tissue-TekOCT, and cryosectioned to a thickness of 18-to-40μm. Sections were fixed in methanol for 5min at −20°C, then washed with PBS. Sections were blocked for 1h in PBS containing 10% donkey serum (DS), then incubated overnight with anti-α2-laminin antibodies in block buffer at 4°C. Sections were then washed with PBS, then incubated for 1h at room temperature with CY3-conjugated secondary antibodies. Sections were then washed with PBS, counterstained with 10μg/ml DAPI in PBS for 10min, and mounted using SlowfadeGold.

Fluorescent immunocytochemistry using paraformaldehyde-fixed sections

Cerebral cortices collected from wildtype or *lama2−/−* littermates at postnatal days 1, 5, and 8 were fixed by submersion for 16–24h in 4% paraformaldehyde (PFA) in PBS at 4°C. Older animals (i.e. 14days and beyond) were anesthetized with Avertin and perfused intracardially with a saline, followed by 4% PFA. Brains were removed and postfixed for 2h in PFA, then equilibrated in 30% sucrose at 4°C. Brains were frozen in OCT using an isopentane-dry ice

bath, and coronal cyrostat sections of 18–25μm were prepared. Sections were blocked in 10% DS with 0.1% Triton-X-100 for 1h before incubating with antibodies overnight at 4°C. Sections were then incubated with Dylight488 or Cy3-secondary antibodies in 10% DS for 1h, followed by DAPI and mounting with SlowfadeGold.

To evaluate laminin immunoreactivity in conjunction with lineage-specific antibodies (as in Fig. 1), brains were dissected from C57Bl/6 mice at P1, followed by immersion fixation in 4%PFA for 8 hours, then cryoprotection in 30% sucrose for 24h, all at 4°C. Brains were frozen in OCT in an isopentane-dry ice bath, and coronal cryostat sections of 25μm prepared. Sections were boiled in Antigen Retrieval Solution pH3 (Dako) for 30min, followed by PBS washes. Immunocytochemistry was then performed as above.

Alternatively, 40μm free-floating sections were prepared (as in Fig. 2C, Fig. S1). Briefly, cryosections were placed in chilled tissue stock solution (30% glycerol:30% ethylene glycol: 10% 0.2M phosphate buffer). For immunodetection, floating sections were washed 3 times in PBS with 0.2% TritonX-100 (PBST). After blocking in 1% DS in PBST for 30min, sections were incubated in antibody overnight at room temperature. Sections were washed with PBST and incubated in fluorescent secondary antibody for 1h. Finally, floating sections were washed 3 times with PBST, followed by 3 washes with 0.1 M phosphate buffer. Sections were then incubated in DAPI for 10min, and mounted with SlowFade Gold.

Analysis of Sox2$^+$ intermediate progenitor cells in the dorsal subventricular zone

Immunocytochemistry with progenitor cell type-specific antigens was performed in conjunction with proliferation and apoptosis markers. PFA-fixed coronal sections were pretreated with 0.3% TritonX-100 detergent in PBS for 15 min at room temperature. Sections were heated at 95–99°C for 20 min in 1XTarget Retrieval Solution citrate buffer (pH 6.0, Dako). Slides were then allowed to cool for 20 min at room temperature. After several washes with PBS, sections were blocked in 10% DS with 0.1% TritonX-100 for 1h. Immunocytochemistry using Sox2 antibody in combination with either nestin (found in radial glia) or PCNA (found in proliferating cells) antibody was performed overnight at 4°C. Sections were washed with PBS then incubated in fluorescence-conjugated secondary antibodies for 1h, before counterstaining with DAPI and mounting with SlowFade Gold. TUNEL assays (ApopTag™ In Situ Apoptosis Detection Kit, Chemicon) were also performed to determine cell death in the Sox2+ population. Sections were imaged using a Zeiss LSM510 Meta confocal microscope with 10x eyepiece magnification using 40x [1.3 numerical aperture(NA), oil], 63x (1.4NA, oil), and 100x (1.4NA, oil) objectives. The density of Sox2$^+$- cells in the dorsal SVZ, along with the numbers of proliferating (PCNA$^+$) Sox2$^+$-cells and apoptotic (TUNEL$^+$) Sox2$^+$-cells, were determined using the Axiovision Rel. 4.8 software (Carl Zeiss, Germany). Morphometric analyses of the thickness of the dorsal SVZ and the distances of Sox2$^+$- and PCNA$^+$Sox2$^+$-immunopositive nuclei from the ventricular surface were done on matching sections of wildtype and *LAMA2−/−* cerebral cortices using the Axiovision Interactive Measurement module.

Analysis of oligodendroglial density, survival, and proliferation

To determine oligodendroglial cell density in the dorsal SVZ and corpus callosum, frozen and PFA-fixed cortical sections (18–25 μm) were blocked in 10% DS with 0.1% TritonX-100 for 1h at room temperature. Immunocytochemistry using anti-Olig2 (all oligodendrocyte lineage stages) in conjunction with either anti-PDGFRα (oligodendrocyte progenitors) or anti-APC (CC1; mature oligodendrocytes) was performed overnight at 4°C. Sections were washed in PBS, then incubated with fluorescence-conjugated secondary antibodies for 1h, before washing again in PBS. The numbers of $Olig2^+$, $PDGFRa^+Olig2^+$ and $CC1^+Olig2^+$ cells in the corpus callosum and the dorsal SVZ were scored in matching sections of wildtype and *lama2−/−* cerebral cortices.

To determine oligodendroglial proliferation and survival, stage-specific antibodies (e.g., NG2+ or CC1+) were used in conjunction with either PCNA antibodies (for proliferating cells) or ApopTag™ In Situ Apoptosis Detection Kit, to detect apoptotic cells. Sections were imaged using Zeiss LSM510 Meta confocal microscope or a Zeiss Axioplan inverted fluorescence microscope fitted with 10x eyepiece magnification using 5x (0.16 NA), 10x (0.3 NA), 20x (0.5 NA), 40x (0.75 NA), and 63x (1.4 NA, oil) objectives. The corpora callosa and the dorsal SVZ of matching sections of wildtype and mutant cortices were analyzed to determine the percentages of proliferating OPCs ($PCNA^+NG2^+$ cells) and apoptotic oligodendroglia ($TUNEL^+$ $NG2^+$ and $TUNEL^+$ $CC1^+$ cells).

Western blot analysis

Minced cerebral cortices collected from age-matched wildtype and *LAMA2−/−* littermates were lysed at 95°C for 10 min, with occasional trituration, in 1% SDS, 20 mM Tris pH 7.4 with protease and phosphatase inhibitor cocktails (Calbiochem). Following centrifugation at 14,000 rpm, the supernatant was collected and used to determine total protein concentration (Bio-Rad). Lysates were then boiled for 5 min in Laemmli solubilizing buffer (LSB) with 4% β-mercaptoethanol (βME). Proteins were separated by SDS-PAGE using 7.5, 12, or 15% acrylamide minigels and transferred onto 0.45 μm nitrocellulose. Membranes were blocked in 0.1%Tween20, and TBS-T containing either 4% bovine serum albumin (BSA) or 1% nonfat milk (blocking buffer) for 1h, followed by antibodies in blocking buffer overnight at 4°C. Membranes were washed in TBS-T, incubated for 1h in HRP-conjugated secondary antibodies (Amersham) diluted 1:3000 in blocking buffer, washed in TBS-T, and then developed using enhanced chemiluminescence (Amersham). Relative densitometries were determined using the NIH ImageJ Processing and Analysis Program.

Electron microscopy and morphometric analysis

21 day old littermate mice were processed for electron microscopy (three *lama2−/−* and two wildtype). Mice were perfused intracardially with 4% paraformaldehyde/2.5% glutaraldehyde in 0.1M phosphate buffered saline. Brains were postfixed overnight at 4°C and individual structures were cut along the sagittal plane on a Leica VT-1000 Vibratome at 50–60 μm. Free-floating sections were placed in 2% osmium tetroxide in 0.1 M phosphate buffer, washed in 0.1M phosphate buffer and dehydrated in a graded series of ethyl alcohol. Sections were then vacuum-infiltrated in Durcupan ACM embedding agent (Electron Microscopy Sciences) overnight, flattened between two pieces of ACLAR film (Ted Pella)

and placed in a 60°C oven for 48–72h to polymerize. Regions of interest were blocked and ultrathin sections (70–80 nm) were generated using a Reichert-Jung 701704 Ultracut E ultramicrotome. Ultrathin sections were placed on formvar-coated copper slot grids and counterstained with uranyl acetate and lead citrate. Samples were viewed with a Tecnai™ Spirit BioTwin G^2 transmission electron microscope (FEI Company). Digital images were acquired with an AMT XR-60 CCD Digital Camera System (Advanced Microscopy Techniques, Corp.) and compiled and analyzed using Adobe Photoshop and ImageJ (NIH). The g-ratio of myelinated axons was determined by dividing the axon diameter by the myelin diameter. A minimum of 387 axons was measured for the corpus callosum of each genotype.

Statistical analysis

Statistical significance of cell density, proliferation, and survival data sets was determined using the Student's two-tailed, paired t-test, except when comparing values between 2 different postnatal timepoints with unequal numbers of animals (unpaired t-test). Graphs depict the mean values, with error bars depicting standard error of the mean. Statistical analyses on intermediate progenitor cell distances from the ventricle surface and g-ratios of myelinated axons were performed using the Mann-Whitney Rank Sum Test (SigmaStat). Box plots depict distances of $Sox2^+$ and proliferating i.e. $PCNA^+Sox2^+$ cells from the ventricle surface in the dorsal SVZ at P1. Statistical significance of the proportion of proliferating $Sox2^+$ cells found within abventricular binned distances was determined using one-way ANOVA (SigmaStat).

Results

Laminins are found in the VZ-SVZ germinal niche at the onset of postnatal gliogenesis

Previous studies have shown that laminins are found throughout the CNS during embryogenesis (Lathia et al., 2007; Libby et al., 2000; Liesi, 1985). In contrast, laminins are restricted in the adult brain, with laminins largely confined to basal lamina of the (1) pia and (2) cerebral vasculature (Villanova et al., 1997). The presence and distribution of laminins during postnatal gliogenesis, however, remain largely uncharacterized. We therefore assessed laminin γ1 immunoreactivity, in conjunction with cell lineage-specific antibodies, at the onset of postnatal gliogenesis i.e postnatal day 1 (P1). We chose to examine laminin γ1 because this subunit is a component of the majority of laminin heterotrimers, including laminin-2 (which has been implicated in CNS myelination). At P1, laminin immunoreactivity was widespread in the developing forebrain, and was particularly prominent in the VZ-SVZ, as well as in vascular basal lamina (Fig. 1, laminin/GFAP top row). At higher magnification, VZ-SVZ laminin was observed in a pericellular distribution and in vascular basal lamina, and was also found in "endfeet" type structures at the ventricle surface (Fig. 1, laminin/GFAP′ row). Many laminin-positive endfeet colocalized with GFAP-positive radial glial processes (within the SVZ, GFAP immunoreactivity detects radial glia, as well as developing stem/progenitors). In addition, Pax6+ cells were found in areas with significant pericellular laminin immunoreactivity, with Pax6+ cells being a mixture of stem and progenitor cells, as well as progenitor cells in areas adjacent to the SVZ (Fig. 1, laminin/Pax6 row). Finally, we observed many PDGFRα+ OPCs in association with

laminin, both within the SVZ as well as in SVZ-adjacent regions (Fig. 1, laminin/PDGFRα rows).

Next, immunohistochemistry was performed to compare laminin levels at P1 and P8 (here using an antibody that detects both the β1 and γ1 laminin subunits). In P1 cerebral cortices, high levels of laminin were detected in the basement membranes of the pia and the vasculature (Supplementary Fig. S1, upper panels). Additionally, moderate pericellular laminin was observed in the marginal zone and other cortical layers. By P8, laminin immunoreactivity in the pia and blood vessels remained comparable to levels observed at P1, however, pericellular immunoreactivity in the cortical layers was less apparent (Supplementary Fig. S1). Pronounced laminin immunoreactivity was detected in basal lamina surrounding the blood vessels of the SVZ at P1, as well as extravascularly throughout the VZ-SVZ particularly near the ventricular surface (Supplementary Fig. S1, lower panels), where the ependymal cells that line the lateral ventricles reside. By P8, VZ-SVZ laminin immunoreactivity continued to be detected in the vascular basal lamina, while extravascular laminin structures were not as pronounced (Supplementary Fig. S1). Overall these findings indicate that stem cells, intermediate progenitors, and newly-born oligodendrocyte lineage-committed progenitor cells are located in proximity to laminins in the VZ-SVZ during early postnatal development.

Laminin regulates the cellular composition of the postnatal VZ-SVZ

To determine whether laminins influenced the structure or function of the postnatal VZ-SVZ gliogenic germinal niche, we evaluated oligodendroglial development in LAMA2−/− mice, which do not express the gene that encodes the laminin α2-subunit, an obligate subunit for a subset of laminin heterotrimers i.e. laminins-2, -4, and -12 (also referred to as laminins-211, -221, and -213). Human LAMA2 mutations have furthermore been shown to cause developmental defects in the CNS that remain largely uncharacterized at the cell/molecular level, but are known to include structural e.g., hypoplasias and agyrias, as well as functional abnormalities e.g., seizures, mental retardation, and white matter hypointensities (Allamand and Guicheney, 2002; Buteică et al., 2008; Leite et al., 2005a; Leite et al., 2005b; Miyagoe-Suzuki et al., 2000; Philpot et al., 1999; Sunada et al., 1995). A hypomorph for laminin α2 expression, the *dy/dy* mouse, was previously found to have CNS myelin abnormalities (oligodendrogenesis, however, was not evaluated).

First, laminin α2 immunohistochemistry was used to verify the absence of laminin α2 in LAMA2−/− mice (Figs.2A,B). Wildtype mice had high levels of laminin α2 in the basal lamina of P1 cerebral cortices (Fig. 2A), and moderate levels within the VZ-SVZ (Fig. 2B). Matched sections obtained from LAMA2−/− mice showed no laminin α2 immunoreactivity (Figs.2A,B). To determine if the absence of laminin α2 influenced the structure or function of the VZ-SVZ germinal niche for oligodendrocytes, a subset of the resident cell types of the VZ-SVZ was assessed. First, morphological analysis of the cell-dense VZ-SVZ by DAPI nuclear staining showed a significant reduction in the average thickness of the dorsal VZ-SVZ in matched cortical sections from LAMA2−/− mice (61.0±6.2μm in LAMA2−/− versus 84.3±12.5μm in wildtype; n=4; p=0.0357). Next, immunohistochemistry on free-floating sections was used to detect the intermediate filament protein nestin (found in radial glia) in

conjunction with the neural progenitor cell transcription factor, Sox2 (Fig. 2C). The two lefthand panels show projected images of 40-μm confocal stacks taken from LAMA2−/− and wildtype littermates. Single plane images (two righthand panels) were also acquired to visualize individual fibers and their attachments, which have an “endfoot” type appearance (Fig. 2C). In wildtype mice, radial glia had a stereotypical palisade arrangement, with their corresponding apical attachments terminating near the lateral ventricle. In LAMA2−/− mice, however, radial glial cell apical processes appeared disorganized, with apical attachment sites less apparent, suggestive of a lack of, or alteration in, radial glial adhesion to structures within the VZ-SVZ (Fig. 2C, inset).

We next examined the composition of stem/progenitor cells found in the early postnatal VZ-SVZ in the absence of LAMA2 expression. First, we assessed $Sox2^+$ cells, as Sox2 is highly expressed in both neural stem cells (NSCs) and intermediate progenitor cells (iPCs). Analyses of $Sox2^+$cell densities at P1 revealed no significant difference, however, between the densities of Sox2+ progenitors in the VZ-SVZ of wildtype and LAMA2−/− mice (Fig. 2D; 1754037.6±145429.4 cells/mm^3 versus 1774479.4±184591.2, respectively, n=3, p=0.919), suggesting that LAMA2−/− mice are able to generate (and maintain) appropriate numbers of NSCs/iPCs. There were also no significant differences in $Sox2^+$ cell densities between wildtype and LAMA2−/− SVZ at both P5 (Fig. 2D; 1469273.6±328582.9 cells/mm^3 compared to 1177243.6±8616.6, respectively, n=3, p=0.347) and P8 (Fig. 2D; 609679.1±32939.8 cells/mm3 in wildtype versus 661025.9±139808.7 in mutant SVZ, n=3, p=0.856), indicating that appropriate numbers of NSCs/iPCs are maintained in the LAMA2−/− mutant VZ-SVZ during these oligodendrogenic stages.

To determine if oligodendrogenesis was affected by the absence of laminin α2, NG2 immunohistochemistry was performed to detect newborn $NG2^+$ OPCs in the SVZ (Figs. 2E,F). At P1, the density of $NG2^+$ OPCs per volume of VZ-SVZ in LAMA2−/− mice was ~60% of wildtype (Fig. 2E; 138346.1±2807.0 cells/mm^3 versus 86196.0±4682.1, respectively, n=4, p=0.0178). By P5, however, the density of $NG2^+$ OPCs in the VZ-SVZ of LAMA2−/− mice had caught up to those in wildtype mice, and by P8, surprisingly, were increased in the VZ-SVZ of LAMA2−/− mice relative to those in control mice (Fig. 2E; 185024.0±28982.2 cells/mm^3 in LAMA2−/− versus 125971.1±24673.5 in wildtype, n=3, p=0.0163). These findings suggested that VZ-SVZ oligodendrogenesis may be dysregulated in the absence of α2-containing laminins.

Laminin regulates the spatial distribution of $Sox2^+$ progenitors in the SVZ

Cell adhesion to the ECM has been shown to regulate both the positioning and proliferation of neural progenitors. For instance, the deletion of the nidogen-binding site of the laminin γ1 chain causes pial basement membrane disruption during embryonic development, leading to radial glial basal endfeet retraction and ectopic positioning of radially-migrating neuroblasts (Halfter et al., 2002). In the adult VZ-SVZ, where proliferating neural progenitor cells (NPCs) associate closely with laminin-rich blood vessels, the administration of integrin blocking antibodies disrupts NPC association with blood vessel basal lamina, altering both NPCs position and proliferation (Shen et al., 2008). It remains unknown, however, whether adhesion regulates CNS progenitors during gliogenesis.

Localized extrinsic signals within the SVZ, such as morphogens (Sonic Hedgehog, Shh) and growth factors (e.g., PDGF) (Bongarzone, 2002), help to regulate gliogenesis. Therefore the location of a progenitor cell within the niche could influence that cell's ability to generate oligodendroglia. To determine whether the positions of progenitors were altered in the VZ-SVZ of LAMA2−/− mice, we measured the distances of $Sox2^+$ and $PCNA^+Sox2^+$ cell bodies from the ventricular surface (VS) (Figs.3A–C). Significant decreases in the median distances of $Sox2^+$ cells from the ventricular surface were observed in the LAMA2−/− VZ-SVZ at P1 (Figs.3A,B; 19.58 μm from the VS; n=1065) compared to the wildtype SVZ (Figs. 3A and 3B; 26.91 μm from the VS; n=1378). By P8, $Sox2^+$ cells were still found significantly closer to the VS in LAMA2−/− VZ-SVZ compared to control animals (data not shown; median distance of 13.86 μm from the VS in mutant SVZ, versus median distance of 25.16 μm from the VS in wildtype SVZ; n=171 and 219, respectively). Similarly, proliferating progenitors ($PCNA^+Sox2^+$) in the LAMA2−/− VZ-SVZ were distributed inappropriately (Figs.3A–C). On average, $PCNA^+Sox2^+$ cells in the LAMA2−/− VZ-SVZ were found significantly closer to the ventricle surface (Figs. 3A and 3B; median distance of 14.74μm from the VS; n=564) compared to their wildtype counterparts (Figs. 3A and 3B; median distance of 29.69 μm from the VS; n=788). Individual cell distance measurements were also grouped into 6 abventricular bins (i.e., <20, 20–40, 60–100, 100–140, 140–180, and >180 μm from the VS), which revealed that an increased proportion of the proliferating progenitors ($PCNA^+Sox2^+$) in the LAMA2−/− SVZ can be found within 20 μm from the VS (Fig. 3C; 59.8% compared to 40.2% in wildtype littermates; $p<0.05$; one-way ANOVA).

Previous studies have provided evidence that adhesion regulates the proliferation of various progenitor cell types in the CNS. In mice lacking β1-integrin in CNS neural cells, for instance, cerebellar granule cell precursors proliferate less (Blaess et al., 2004). To examine if progenitor proliferation is affected by the loss of laminin α2, we determined the percentage of proliferative OPCs and iPCs in the VZ-SVZ of wildtype and LAMA2−/− mice (Fig. 3D). Although LAMA2−/− mice have fewer resident OPCs in the P1 VZ-SVZ (Fig. 2E), we found no significant differences in the proportion of $PCNA^+$ cells within the $NG2^+$ OPC populations of LAMA2−/− and wildtype VZ-SVZ (Fig. 3D; 37.1±6.9% versus 48.8±14.9%, respectively, n=3, p=0.328), with in fact a slightly higher percentage of proliferative NG2+ cells being found in the LAMA2−/− VZ-SVZ. Analysis of later timepoints also revealed no significant differences in OPC proliferation between control and LAMA2−/− mice (Fig. 3D; at P5, 27.1±4.1% in controls versus 33.5±7.0% in mutants, n=3, p=0.576; at P8, 48.5±1.5% in controls compared to 34.6±12.8% in mutants, n=3, p=0.394). $Sox2^+$ progenitors in the LAMA2−/− SVZ had similar levels of proliferation to that seen in control mice, as determined by the percentage of $PCNA^+$ cells within the $Sox2^+$ progenitor pool (Figs.3D; at P1, 51.7±17.6% in wildtype versus 54.9±3.6% in LAMA2−/− mice; n=3; p=0.870; at P5, 41.2±1.5% in controls versus 31.1±2.3% in mutants, n=3, p=0.335; at P8, 33.0±5.6% in controls compared to 24.7±3.9% in mutants, n=3, p=0.138). Together these data indicate that the absence of laminin α2 significantly disturbs the organization and positioning of Sox2+ progenitor cells in the VZ-SVZ, and, while progenitor cells proliferate in an abnormal location, proliferation of both Sox2+ intermediate progenitors and NG2+ OPCs occurs, surprisingly, to the same degree.

Laminin inhibits oligodendrocyte progenitor cell death in the SVZ

Given that fewer NG2$^+$ OPCs were found in the dorsal SVZ of LAMA2−/− mice, we tested the possibility that OPCs produced in the VZ-SVZ of LAMA2−/− mice die more readily compared to those in their wildtype littermates. We performed TUNEL to detect dying cells, in conjunction with either NG2 or Sox2 immunohistochemistry, on cortical sections from wildtype and LAMA2−/− mice (Fig. 4). A large increase in the percentage of TUNEL+ cells was observed within NG2$^+$ OPCs in the LAMA2−/− VZ-SVZ at P1, relative to that in wildtype (Figs.4A,B; 64.85±7.3% in LAMA2−/− VZ-SVZ; 31.4±3.3% in wildtype, n=3, p=0.0245). No significant differences in OPC death were detected at postnatal days 5 and 8, however (Fig. 4B). In contrast, no differences were observed in Sox2$^+$ progenitor cell death at any age (Fig. 4C), suggesting that, despite their aberrant location, Sox2$^+$ intermediate progenitor cells survived appropriately in the LAMA2−/− VZ-SVZ. Together, these findings indicated that changes in OPC survival, but not OPC proliferation, plays a major role in altering the numbers of OPCs in the SVZ of LAMA2−/− mice.

Laminin regulates the number of oligodendrocyte progenitors in developing white matter

Since LAMA2−/− mice had fewer OPCs at their site of genesis in the VZ-SVZ, we next examined whether the OPC population in the overlying white matter tract, the corpus callosum, was similarly affected (Fig. 5). Significantly fewer NG2$^+$ OPCs per volume were found in the developing corpus callosum of LAMA2−/− mice compared to wildtype mice at P1 (Figs.5A,B; 106363.9± 2807.0 cells per mm^3 in wildtype; 57227.5± 4346.6 cells per mm^3 in LAMA2−/−; n=3; p=0.00757). Western blots revealed that NG2 protein levels were consistently lower in cerebral cortical lysates from P1 LAMA2−/− mice compared to wildtype (Fig. 5C). As expected, the density of NG2$^+$ cells in both wildtype and LAMA2−/− corpus callosum had increased by P5 (Fig. 5A). However, while wildtype mice had an approximately 48% increase in NG2$^+$ cell density from P1 to P5 (Fig. 5A; 106363.9± 2807.0 cells per mm^3 at P1; 157416.6 ± 13633.7 cells per mm^3 at P5; n=3; p=0.0469), LAMA2−/− mice had an almost two-fold increase in NG2$^+$ cell density within the same developmental period (Fig. 5A; 57227.5± 4346.6 cells per mm^3 at P1; 110329.9± 4057.4 cells per mm^3 at P5; n=3; p=0.00338). By postnatal day 8, however, NG2$^+$ cell densities in the LAMA2−/− corpus callosum remained significantly decreased compared to control animals (Fig. 5A; 133529.3 ± 13047.4 cells per mm^3 in wildtype; 93890.4 ± 7317.2 cells per mm^3 in knockout; n=3; p=0.0447). These findings indicated that laminin α2 is critical for generating, or possibly maintaining, the correct number of OPCs to populate the developing corpus callosum.

NG2 immunohistochemistry reveals cell processes, which can be difficult to assign to cell bodies once myelination is underway; we therefore used a second approach to examine OPC density in the developing corpus callosum from birth through myelination. Here we examined the densities of cells positive for both Olig2 and PDGFRα. During early postnatal development i.e. P0/1 through P8, PDGFRα$^+$Olig2$^+$ cell densities in the LAMA2−/− corpus callosum were consistently lower than wildtype densities (Fig. 5D). For instance, at P5, LAMA2−/− mice had ~33% fewer PDGFRα$^+$Olig2$^+$ OPCs compared to control littermates (Fig. 5D; 77288.8±10169.0 cells per mm^3 in wildtype; 51664.1±2581.5 cells per mm^3 in P5 LAMA2−/−; n=3, p=0.0130). This significant reduction in the density of PDGFRα$^+$Olig2$^+$

OPCs in the LAMA2−/− corpus callosum persisted until P8 (Fig. 5D; 66494.8±5720.4 cells per mm^3 in wildtype; 51866.7±2581.5 cells per mm^3 in P8 LAMA2−/−; n=3, p=0.0433). Beyond P8, however, the density of PDGFRα$^+$Olig2$^+$ cells in the LAMA2−/− corpus callosum continued to increase such that by P21, OPC densities were significantly higher, approximately two-fold, compared to wildtype (Fig. 5D; 32469.9±1843.5 cells per mm^3 in wildtype; 67168.7±6608.6 cells per mm^3 in P21 LAMA2−/−; n=3, p=0.0365). By P28, OPC densities in the corpus callosum of both wildtype and LAMA2−/− mice had decreased, presumably due to OPC differentiation, although the LAMA2−/− corpus callosum continued to retain more PDGFRα$^+$Olig2$^+$ OPCs relative to control littermates (Fig. 5D; 37252.4±3006.7 cells per mm^3 in P28 LAMA2−/−; 21681.6±2015.6 cells per mm^3 in control; n=3, p=0.00438). Overall, the lower density of OPCs (defined as either NG2$^+$ or PDGFRα$^+$Olig2$^+$) during the peak of cortical oligodendrogenesis was followed by a progressive elevation of OPC density later during development, suggesting that OPC production is initially delayed, but that OPCs begin to accumulate during myelination onset in LAMA2−/− mice.

Since LAMA2−/− mice had abnormally low OPC densities during the perinatal period, we next sought to determine if increased OPC apoptosis and/or reduced OPC proliferation within the corpus callosum contributed to this OPC deficit. TUNEL in conjunction with NG2 immunohistochemistry was performed to detect apoptotic OPCs in the corpus callosum of LAMA2−/− and control littermates (Figs.5E,F). At P1, higher percentages of TUNEL$^+$ OPCs were observed in LAMA2−/− mice compared to wildtype (Fig. 5E; 14.2± 2.3% in wildtype; 24.5± 3.4% in P1 LAMA2−/−; n=5; p=0.0492). A small increase in OPC death was also found in the P5 LAMA2−/− corpus callosum relative to control littermates (Fig. 5E; 10.9± 0.9% in wildtype; 12.5± 1.0% in P5 LAMA2−/−; n=3; p= 0.0130). By P8, however, OPC death in both wildtype and LAMA2−/− corpus callosum was similar between genotypes (Fig. 5E; 14.8±0.8% in wildtype; 12.8±4.7% in P8 LAMA2−/−; n=3, p=0.742). These results indicated that increased levels of OPC death occur in the early postnatal corpus callosum LAMA2−/− mice. However, the level of OPC death was not as pronounced as what was seen in the SVZ (Fig. 4B).

Proliferation was also analyzed in callosal OPCs, using PCNA and NG2 immunohistochemistry to determine the percentage of proliferating OPCs within the total OPC pool (Fig. 5G). While fewer OPCs were found in the corpora callosa of LAMA2−/− mice (Figs.5A,D), the percentages of these OPCs that were proliferative i.e. PCNA$^+$, were similar to those in control (Fig. 5G; at P1, 37.0±7.9% in wildtype; 52.8±2.2% in LAMA2−/−, p=0.200; at P5, 60.4±6.1% in wildtype; 58.5±7.7% in LAMA2−/−, p=0.879; at P8, 50.5±2.2% in wildtype, 50.2±5.5% in LAMA2−/−; n=3). Thus, altered OPC proliferation is unlikely to contribute to the observed differences in OPC density. Overall, these results indicate that early in postnatal development, α2-containing laminins are critical for generating an adequate supply of OPCs to populate the developing corpus callosum in two ways: (1) by promoting the survival of newborn OPCs in the germinal niche of the VZ-SVZ, and (2) by promoting the survival of OPCs within the callosum itself. Later in postnatal development, however, OPC survival becomes laminin-independent.

Laminin regulates oligodendrocyte maturation

Given that LAMA2−/− mice had higher than normal OPC densities during the peak of myelination e.g. P21, we next examined whether OPC maturation was deficient. The density of mature oligodendrocytes in the corpus callosum was determined by assessing the number of cells per volume that were double-positive for CC1 and Olig2 (Figs.6A,C). During early postnatal development, LAMA2−/− mice have significantly fewer callosal OPCs than do their wildtype littermates (Figs.5A,D). When cortical myelination begins at P8, LAMA2−/− mice also have fewer (~56% less) mature oligodendrocytes in their corpora callosa compared to wildtype littermates (Fig. 6C; 16706.5±2376.6 cells per mm^3 in LAMA2−/−; 38059.1±4658.7 cells per mm^3 in wildtype; n=3; p=0.0214). As myelination proceeds between P8 and P14, $CC1^+Olig2^+$ cell densities increased significantly in both wildtype and LAMA2−/− mice. By 2 weeks of age, there were no significant differences in mature oligodendrocyte density between wildtype and LAMA2−/− mice (Fig. 6C; 87475.9±5603.7 cells per mm^3 in wildtype; 75579.5±10254.0 cells per mm^3 in LAMA2−/−; n=4; p=0.227). These findings indicated that reduced OPC densities correlated with lower densities of mature oligodendrocytes in the *early* postnatal LAMA2−/− corpus callosum.

Since by P21 LAMA2−/− mice had higher than normal OPC densities, we next evaluated the densities of mature oligodendrocytes in 2–4 week old LAMA2−/− mice to determine if oligodendrocyte differentiation at these later timepoints was also impaired (Figs.6C). As myelination proceeds, the densities of $PDGFR\alpha^+Olig2^+$ OPCs decreased steadily in wildtype mice (Fig. 5D) while the density of $CC1^+Olig2^+$ mature oligodendrocytes increased concurrently (Fig. 6C). We found that from P14 to P28, the densities of $CC1^+Olig2^+$ cells doubled in the corpora callosa of controls (Fig. 6C; at P14, 87475.9±5603.7 cells per mm^3; 167927.6±32167.5 cells per mm^3 at P28; n=3–4; p=0.0337). In LAMA2−/− corpora callosa, however, the densities of mature oligodendrocytes did not change significantly between P14 and P28 (Fig. 6C; n=3–4), *in spite of* the presence of excess OPCs (Fig. 5D). Beyond P14, $CC1^+Olig2^+$ cell densities remained significantly lower in the LAMA2−/− corpus callosa compared to controls (Fig. 6C; at P21, 89705.9±24402.4 cells per mm^3 in LAMA2−/−; 130612.84±22473.3 cells per mm^3 in wildtype; n=4; p=0.0184). At P28, wildtype mice had ~2.5-fold more mature oligodendrocytes ($CC1^+Olig2^+$ cells) than their LAMA2−/− littermates (Fig. 6C; 167927.6±32167.5 cells per mm^3 in wildtype; 65891.0±7728.7 cells per mm3 in LAMA2−/− mice; n=3, p=0.0634). To confirm these changes in oligodendrocyte differentiation, Western blots were used to detect levels of oligodendrocyte stage-specific proteins in cortical lysates from P21 wildtype and LAMA2−/− mice (Fig. 6B). Myelin basic protein (MBP) and 2′, 3′-cyclic nucleotide 3′-phosphodiesterase (CNP), proteins found in differentiated oligodendrocytes, were detected at decreased levels in LAMA2−/− cerebral cortical lysates compared to lysates from wildype littermates (Fig. 6B). Levels of the OPC protein NG2, on the other hand, were elevated in lysates from P21 LAMA2−/− cortices, compared to wildtype (Fig. 6B). Overall, the decreased densities of mature oligodendrocytes, accompanied by abnormally high densities of OPCs, indicated that oligodendrocyte maturation was altered in LAMA2−/− developing white matter. Additionally, low levels of oligodendrocytes could reflect increased cell death in these cells. TUNEL in conjunction with CC1 immunohistochemistry revealed, however, that

oligodendrocytes in LAMA2−/− white matter were no more likely to undergo apoptosis than those in the white matter of wildtype littermates. Overall, oligodendrocyte death was very low in both genotypes at P21 (0.57±0.34% $TUNEL^+$ oligodendrocytes of wildtype, and 1.29±0.73% $TUNEL^+$ oligodendrocytes in LAMA2−/− mutants; n=3, p=0.537). At P28, however, *no* $TUNEL^+CC1^+$ cells were detected in either genotype. Finally, to assess the degree of newly-formed oligodendrocytes within the CC1+ oligodendrocyte pool, BrdU was injected into mice at P8 to track the presence of BrdU in CC1+ oligodendrocytes at 24 hours post-injection. A significantly decreased percentage of BrdU+ CC1+ cells was observed in LAMA2−/− corpus callosum compared to that in wildtype littermate controls (3.58±1.19% in LAMA2−/−; 9.86±1.93% in WT; n=4, p=0.0158), indicative of fewer *newly-generated* oligodendrocytes in the LAMA2−/− corpus callosum. At later stages i.e. P14, using the same 24 hour injection paradigm, the decrease in the percentage of CC1+ cells that were also BrdU positive was less pronounced (1.54±0.07% in LAMA2−/− versus 4.94±2.48% in WT; n=4, p=0.0694).

Laminin regulates myelination

Since the corpus callosum of P21 LAMA2−/− mice contained fewer oligodendrocytes, we next examined myelin itself (Fig. 7). Immunohistochemistry to detect MBP, as well as neurofilament to detect axons, was used to examine the gross organization of the the corpus callosum in P21 LAMA2−/− and wildtype littermates (Fig. 7A, top panels). Overall, the organization of MBP+ fibers in LAMA2−/− callosa were comparable to those in wildtype, but often appeared more sparse (Fig. 7A, top). The corpora callosa of LAMA2−/− mice were also thinner compared to those in their wildtype littermates (Fig7A; 186.5±15.1 μm in LAMA2−/−; 242.4±9.4 μm in wildtype; n=4; p=0.0240). Axonal organization appeared grossly normal, as visualized by neurofilament immunocytochemistry (not shown). Next, myelin ultrastructure was evaluated using transmission electron microscopy of the P21 corpus callosum (Figs.7A–C). Analysis of electron micrographs revealed that axons in LAMA2−/− mice had thinner myelin compared to those in their wildtype counterparts (Figs. 7A, bottom panels). When individual g-ratios were plotted as a function of axon diameter (Fig. 7C), significant increases were observed in the median g-ratio in the mutant corpus callosum (0.822; 567 axons, $p<0.001$) compared to wildtype corpus callosum (0.755; 387 axons). Axonal g-ratios were also binned by axon diameter, revealing that axons of all sizes in the corpus callosum had significantly thinner myelin (Fig. 7B). Analyses of both overall axon density and axonal size distribution, however, showed that there were no significant differences in these parameters between wildtype and LAMA2−/− corpora callosa (not shown). Together these data reveal that defects in oligodendrogenesis in the VZ-SVZ, combined with defects in oligodendrocyte maturation in the corpus callosum, lead to defects in myelination in LAMA2−/− mice.

Discussion

Extracellular matrix proteins found in germinal niches have been implicated in regulating neurogenesis in the developing embryo as well as in the adult brain. In contrast, little is known regarding a potential role for extracellular matrices in regulating gliogenesis. In the current study, we found that oligodendrogenesis in the perinatal VZ-SVZ depended on

laminin extracellular matrix proteins such that mice that lack expression of the laminin α2 subunit (LAMA2−/−) had fewer OPCs. We furthermore identified defects in the spatial organization of intermediate progenitor cells in the LAMA2−/− perinatal VZ-SVZ niche, coupled with inappropriately high levels of death within newly-born VZ-SVZ OPCs. This deficit in VZ-SVZ OPCs resulted in fewer OPCs in an adjacent white matter tract, the corpus callosum, which also had inappropriately high levels of OPC death perinatally, followed by defective oligodendrocyte maturation and myelination. Together, these findings indicate that laminin regulates both VZ-SVZ progenitor cells and oligodendrocytes in the developing cerebral cortex, and may therefore have two sites of action: (1) in the VZ-SVZ, where laminins regulate the survival of newly-born OPCs (as summarized in Fig. 8), and, (2) in the emerging white matter, where axon-associated laminins regulate OPC survival in addition to oligodendrocyte maturation/myelination.

Previous studies of *dy/dy* mice, a hypomorph with a laminin α2 deficiency, had revealed that decreased laminin levels resulted in reduced levels of myelination and oligodendrocyte maturation in the adult CNS, however, these studies did not address a possible role for laminin in oligodendrogenesis itself (Chun et al., 2003; Relucio et al., 2009). In addition, since the precise mutation causing the laminin α2 deficiency in *dy/dy* mice has remains unidentified (Sunada et al., 1994), analyses of oligodendrocyte lineage cells and myelin in *dy/dy* mice were restricted to beyond P21, when mice displayed the characteristic muscular dystrophy that distinguished them from their wildtype littermates. In the current study, by using laminin α2 gene knockout mice, we were able to examine oligodendrocyte differentiation during perinatal and early postnatal development, and identify a novel role for laminin, that of ensuring the survival of newly-born OPCs emerging from the VZ-SVZ germinal niche.

Laminins, radial glial cells, and intermediate progenitors of the VZ-SVZ

Radial glial cells generate intermediate progenitors that give rise to neurons and glia in the developing CNS (Fishell and Kriegstein, 2003; Götz and Barde, 2005; Götz et al., 2002; Sessa et al., 2008). Apical and basal attachments allow radial glial cells to span the developing cortical plate and provide discrete pathways for progenitors migrating out of the VZ (Goldman, 1995; Marshall et al., 2003; Rakic, 2003). Indeed, during embryonic development (i.e. at E16), LAMA2−/− brains were found to have a higher percentage of radial glia with detached apical process; these defects correlated with elevated levels of proliferative neuronal precursor cells in the intermediate zone of the developing cortical plate (Loulier et al., 2009). In the current study, by examining the early postnatal brain, we found that laminins are present both within the VZ-SVZ and the pial basal lamina, suggesting that laminin α2 may continue to influence radial glial cells and their progeny during gliogenesis. Indeed, the radial glial cells in LAMA2−/− mice at birth appeared disorganized, with apical attachment sites at the ventricular surface frequently difficult to detect, reminiscent of the disruptions observed by Loulier and colleagues during embyrogenesis (Fig. 2C, inset). We furthermore found that proliferative Sox2+ cells (a mixture of stem and intermediate progenitor cells) were located abnormally close to the ventricular surface. One possibility therefore is that, due to disruption in the radial glial scaffold of the LAMA2−/− neocortex, $Sox2^{+}$ progenitors take longer to migrate out of the

VZ-SVZ and thus are disproportionately found near the ventricle surface. However, given that OPC densities eventually normalize in the LAMA2−/− corpus callosum, and later on exceed the densities of those found in wildtype, OPCs are clearly able to migrate out of the LAMA2−/− germinal niche to reach the corpus callosum. In fact, OPCs generated in vitro from LAMA2−/− stem/progenitor-derived neurospheres did not have inherent defects in migration (not shown). Interestingly, in contrast to what was observed during neurogenesis (Loullier et al. 2010), the percentages of progenitors that were proliferative in the perinatal gliogenic period of remained unchanged in LAMA2−/− mice, both in the $Sox2^+$ stem/intermediate progenitor population as well as in newly-born NG2+ OPCs. This distinction may reflect inherent differences during neurogenesis versus gliogenesis as to whether proliferation depends on ECM-mediated cell attachment and positioning within the VZ-SVZ.

During neurogenesis, the position of dividing progenitors in the VZ/SVZ also can determine the fate of daughter cells. Upon dividing, apical progenitors in contact with the ventricular surface typically generate a progenitor and a postmitotic daughter neuron. Basally-located progenitors, in contrast, do not contact the ventricle and, at least during corticogenesis, only generate neurons upon division (Cappello et al., 2006; Gotz and Huttner, 2005; Miyata et al., 2004; Noctor et al., 2004). Since LAMA2−/− mice have fewer OPCs at birth, it is possible that aberrant $Sox2^+$ progenitor cell positioning correlates with a failure in fate determination, i.e. in oligodendroglial specification. However, $Olig2^+$ cell densities in the VZ-SVZ of LAMA2−/− mice were comparable to densities in wildtype (not shown), suggesting that oligodendroglial lineage cells were specified at normal rates. Thus, since the onset of NG2 expression occurs later than that of Olig2 (Nishiyama, 2007; Nishiyama et al., 2009), it is more likely that LAMA2−/− mice have a deficit or delay within the early OPC population itself, rather than a failure to generate appropriate levels of $Olig2^+$ intermediate progenitor cells.

Laminin-mediated survival of OPCs in the SVZ

As discussed, several potential mechanisms could explain a reduction in SVZ OPCs. Decreased proliferation was ruled out as a cause in lower numbers, however, as $NG2^+$ cells in both the SVZ and the developing white matter of LAMA2−/− mice had normal percentages that were $PCNA^+$. Also, given that $Olig2^+$ cells were present at normal densities, it remains unlikely that failed oligodendroglial lineage specification accounted for the OPC deficit observed in perinatal LAMA2−/− mice. There was, however, an almost two-fold increase in OPC death in the LAMA2−/− SVZ compared to that in wildtype littermates (Fig. 4).

Appropriate developmental apoptosis has previously is known to be critical to establishing the correct numbers of neuronal progenitors. For instance, in Bcl-X_L-, caspase 3-, and caspase 9-null mice, the genetic deletion of programmed cell death effectors resulted in the accumulation of supernumerary neurons, distortion of cortical structures, and premature lethality (Kuida et al., 1998; Kuida et al., 1996; Roth et al., 2000). In addition, even small increases in cell death within germinal zones can also have profound effects on the developing brain. *In vivo* lineage tracing studies showed that the death of a single VZ-SVZ

cell potentially translates to the loss of hundreds of downstream lineage-restricted progenitors (Levison et al., 1999; Walsh and Cepko, 1988). In LAMA2−/− mice, the two-fold increase in the percentage of dying OPCs in the SVZ germinal niche is therefore a significant cause for decreased OPC densities both in the SVZ and in the adjacent corpus callosum. A decreased ability of $Olig2^+$ intermediate progenitors to generate $NG2^+$ OPCs cannot be ruled out however, but appears unlikely to be the principal reason underlying lower OPC densities.

What is causing OPCs in the LAMA2−/− SVZ to die more readily? Later in development, laminin-mediated signaling promotes the target-dependent survival of early oligodendrocytes in developing white matter in response to limited amounts of trophic factors (Benninger et al., 2006; Colognato et al., 2002). In addition, α6β1 integrin, a laminin receptor, has been implicated in promoting neurosphere maintenance and survival (Campos et al., 2004; Leone et al., 2005), suggesting that laminin-integrin signals may *directly* regulate the survival of newly-born OPCs in the SVZ. However, ventricle-associated ECM-structures called fractones can capture growth factors and regulate growth factor availability in the adult VZ-SVZ (Kerever et al., 2007), and thus it may be that laminins in the perinatal VZ-SVZ similarly localize trophic molecules, and thus *indirectly* regulate cell survival Although newly-formed oligodendrocytes in culture are highly sensitive to laminin as a pro-survival cue (Colognato et al., 2002; Colognato et al., 2004; Frost et al., 1999), laminin does not seem to be required for the survival of cultured OPCs. This observation makes it more likely that laminins in the perinatal VZ-SVZ regulate OPC survival *indirectly* by regulating the availability of as yet unknown pro-survival molecules in the VZ-SVZ microenvironment. As Shh has been found to promote OPC survival in the postnatal SVZ, and laminins have previously been shown to modulate cerebellar granule cell proliferation by binding to Shh (Blaess et al., 2004), one possibility is that laminins modulate SVZ OPC survival by regulating Shh availability within the SVZ (Machold et al., 2003).

An additional point is that no change in survival was detected in $Sox2^+$ intermediate progenitor cells in the LAMA2−/− SVZ, indicating that increased death is likely to be selective for newborn OPCs. Indeed, perinatal OPCs have been shown to be exquisitely sensitive, more so than stem populations, to pro-death stimuli, including hypoxia and chemotherapeutics (Dietrich et al., 2006; Romanko et al., 2004; Rothstein and Levison, 2005). In perinatal LAMA2−/− mice, we propose that needed pro-survival signals for newly-born OPCs found in the VZ-SVZ microenvironment are disrupted, either as a result of altered trophic factor availability and/or direct loss of adhesive interactions between laminins and progenitors, with the former being most likely.

Laminin and oligodendrocyte development in white matter tracts

LAMA2−/− mice had fewer OPCs and fewer mature oligodendrocytes in the early postnatal corpus callosum. By P21, however, corpus callosum in LAMA2−/− mice had elevated OPC densities relative to those in wildtype littermates, suggesting that (1) initial deficits in generating appropriate numbers of OPCs were overcome, and (2) OPCs may accumulate due to impaired oligodendroglial maturation, as was observed previously in laminin-deficient *dy/dy* mice. Thus the increased densities of OPCs in the LAMA2−/− corpus callosum by

P21 indicated that the observed reduction in mature oligodendrocytes cannot be due to a failure of OPCs to arrive at their target white matter destination. Indeed, while oligodendrocyte densities in both wildtype and LAMA2−/− mice increased over time, the density of oligodendrocytes remained lower in the LAMA2−/− corpus callosum, with the spread between wildtype and LAMA2−/− densities growing *more* pronounced with age. Concurrently, the delay in oligodendrocyte maturation correlated with thinner myelin on the axons of the corpus callosum, as observed previously in laminin-deficient *dy/dy* mice (Chun et al., 2003; Relucio et al., 2009). Interestingly, NG2+ cell densities were also lower in LAMA2−/− cortical gray matter (not shown), indicating that oligodendroglial deficits affect multiple regions.

In summary, we have identified a new role for CNS laminins, that of regulating OPC production from the VZ-SVZ germinal niche during postnatal development. This finding indicates that, like the adult brain where the spatial arrangement of cells in contact with extracellular matrix molecules is thought to influence the phenotype of VZ-SVZ stem and/or progenitor cells, the adhesive proteins found in the “gliogenic niche” of the perinatal VZ-SVZ are important for both for the spatial arrangement of progenitors *within* the niche as well as the progenitor output *from* the niche. Future studies will be of interest to determine whether laminins act merely as spatial organizers for other molecules or whether laminins directly modulate cell phenotype through laminin receptors expressed on newly-born OPCs.

Supplementary Material

Refer to Web version on PubMed Central for supplementary material.

Acknowledgments

This study was supported by the National Institute of Neurological Disorders and Stroke (NS054042), the National Multiple Sclerosis Society (RG4357A2), and by the Empire State Stem Cell Fund (NY State Department of Health contract CO26400). The authors wish to thank members of the Colognato lab for helpful discussions, in particular Freyja McClenahan for advice and technical assistance, as well as Susan Van Horn of the Stony Brook CMIC facility for TEM sample preparation and Dr. Bruce Patton (Oregon Health and Science University) for technical advice with LAMA2−/− mice.

References

Allamand V, Guicheney P. Merosin-deficient congenital muscular dystrophy, autosomal recessive (MDC1A, MIM# 156225, LAMA2 gene coding for α2 chain of laminin). European Journal of Human Genetics. 2002; 10:91–94. [PubMed: 11938437]

Benninger Y, Colognato H, Thurnherr T, Franklin RJM, Leone DP, Atanasoski S, Nave K-A, ffrench-Constant C, Suter U, Relvas JB. β1-integrin signaling mediates premyelinating oligodendrocyte survival but is not required for CNS myelination and remyelination. The Journal of Neuroscience. 2006; 26:7665–7673. [PubMed: 16855094]

Blaess S, Graus-Porta D, Belvindrah R, Radakovits R, Pons S, Littlewood-Evans A, Senften M, Guo H, Li Y, Miner JH, Reichardt LF, Müller U. β1-Integrins are critical for cerebellar granule cell precursor proliferation. The Journal of Neuroscience. 2004; 24:3402–3412. [PubMed: 15056720]

Bongarzone ER. Induction of oligodendrocyte fate during the formation of the vertebrate neural tube. Neurochemical Research. 2002; 27:1361–1369. [PubMed: 12512941]

Buteică E, Roşulescu E, Burada F, Stănoiu B, Zăvăleanu M. Merosin-deficient congenital muscular dystrophy type 1A. Romanian Journal of Morphology and Embryology. 2008; 49:229–233. [PubMed: 18516331]

Campos LS, Leone DP, Relvas JB, Brakebusch C, Fässler R, Suter U, ffrench-Constant C. β1 integrins activate a MAPK signalling pathway in neural stem cells that contributes to their maintenance. Development. 2004; 131:3433–3444. [PubMed: 15226259]

Cappello S, Attardo A, Wu X, Iwasato T, Itohara S, Wilsch-Brauninger M, Eilken HM, Rieger MA, Schroeder TT, Huttner WB, Brakebusch C, Gotz M. The Rho-GTPase cdc42 regulates neural progenitor fate at the apical surface. Nature Neuroscience. 2006; 9:1099–1107. [PubMed: 16892058]

Chun SJ, Rasband MN, Sidman RL, Habib AA, Vartanian T. Integrin-linked kinase is required for laminin-2–induced oligodendrocyte cell spreading and CNS myelination. The Journal of Cell Biology. 2003; 163:397–408. [PubMed: 14581460]

Colognato H, Baron W, Avellana-Adalid V, Relvas JB, Evercooren AB-V, Georges-Labouesse E, ffrench-Constant C. CNS integrins switch growth factor signalling to promote target-dependent survival. Nature Cell Biology. 2002; 4:833–841. [PubMed: 12379866]

Colognato H, Ramachandrappa S, Olsen IM, ffrench-Constant C. Integrins direct Src family kinases to regulate distinct phases of oligodendrocyte development. The Journal of Cell Biology. 2004; 167:365–375. [PubMed: 15504915]

Dietrich J, Han R, Yang Y, Mayer-Proschel M, Noble M. CNS progenitor cells and oligodendrocytes are targets of chemotherapeutic agents in vitro and in vivo. Journal of Biology. 2006; 5:22. [PubMed: 17125495]

Fishell G, Kriegstein AR. Neurons from radial glia: the consequences of asymmetric inheritance. Current Opinion in Neurobiology. 2003; 13:34–41. [PubMed: 12593980]

Frost EE, Buttery PC, Milner R, ffrench-Constant C. Integrins mediate a neuronal survival signal for oligodendrocytes. Current Biology. 1999; 9:1251–1254. S1251. [PubMed: 10556090]

Fujii Y, Sugiura C, Fukuda C, Maegaki Y, Ohno K. Sequential neuroradiological and neurophysiological studies in a Japanese girl with merosin-deficient congenital muscular dystrophy. Brain and Development. 2011; 33:140–144. [PubMed: 20303224]

Goldman J. Lineage, migration, and fate determination of postnatal subventricular zone cells in the mammalian CNS. Journal of Neuro-Oncology. 1995; 24:61–64. [PubMed: 8523077]

Götz M, Barde YA. Radial glial cells: defined and major intermediates between embryonic stem cells and CNS neurons. Neuron. 2005; 46:369–372. [PubMed: 15882633]

Götz M, Hartfuss E, Malatesta P. Radial glial cells as neuronal precursors: a new perspective on the correlation of morphology and lineage restriction in the developing cerebral cortex of mice. Brain Research Bulletin. 2002; 57:777–788. [PubMed: 12031274]

Gotz M, Huttner WB. The cell biology of neurogenesis. Nature Reviews Molecular Cell Biology. 2005; 6:777–788. [PubMed: 16314867]

Halfter W, Dong S, Yip YP, Willem M, Mayer U. A critical function of the pial basement membrane in cortical histogenesis. The Journal of Neuroscience. 2002; 22:6029–6040. [PubMed: 12122064]

Iwao M, Fukada S, Harada T, Tsujikawa K, Yagita H, Hiramine C, Miyagoe Y, Takeda S, Yamamoto H. Interaction of merosin (laminin 2) with very late activation antigen-6 is necessary for the survival of CD4+ CD8+ immature thymocytes. Immunology. 2000; 99:481–488. [PubMed: 10792494]

Kang W, Wong L, Shi S, Hébert J. The transition from radial glial to intermediate progenitor cell is inhibited by FGF signaling during corticogenesis. The Journal of Neuroscience. 2009; 29:14571–14580. [PubMed: 19923290]

Kazanis I, Lathia JD, Vadakkan TJ, Raborn E, Wan R, Mughal MR, Eckley DM, Sasaki T, Patton B, Mattson MP, Hirschi KK, Dickinson ME, ffrench-Constant C. Quiescence and activation of stem and precursor cell populations in the subependymal zone of the mammalian brain are associated with distinct cellular and extracellular matrix signals. The Journal of Neuroscience. 2010; 30:9771–9781. [PubMed: 20660259]

Kerever A, Schnack J, Vellinga D, Ichikawa N, Moon C, Arikawa-Hirasawa E, Efird JT, Mercier F. Novel extracellular matrix structures in the neural stem cell niche capture the neurogenic factor fibroblast growth factor 2 from the extracellular milieu. Stem Cells. 2007; 25:2146–2157. [PubMed: 17569787]

Kuida K, Haydar TF, Kuan CY, Gu Y, Taya C, Karasuyama H, Su MSS, Rakic P, Flavell RA. Reduced apoptosis and cytochrome c-mediated caspase activation in mice lacking caspase 9. Cell. 1998; 94:325–337. [PubMed: 9708735]

Kuida K, Zheng TS, Na S, Kuan CY, Yang D, Karasuyama H, Rakic P, Flavell RA. Decreased apoptosis in the brain and premature lethality in CPP32-deficient mice. Nature. 1996; 384:368–372. [PubMed: 8934524]

Lathia JD, Patton B, Eckley DM, Magnus T, Mughal MR, Sasaki T, Caldwell MA, Rao MS, Mattson MP, ffrench-Constant C. Patterns of laminins and integrins in the embryonic ventricular zone of the CNS. The Journal of Comparative Neurology. 2007; 505:630–643. [PubMed: 17948866]

Leite CC, Lucato LT, Martin MGM, Ferreira LG, Resende MBD, Carvalho MS, Marie SKN, Jinkins JR, Reed UC. Merosin-deficient congenital muscular dystrophy (CMD): a study of 25 Brazilian patients using MRI. Pediatric Radiology. 2005a; 35:572–579. [PubMed: 15750812]

Leite CC, Reed UC, Otaduy MCG, Lacerda MTC, Costa MOR, Ferreira LG, Carvalho MS, Resende MBD, Marie SKN, Cerri GG. Congenital muscular dystrophy with merosin deficiency: 1H MR spectroscopy and diffusion-weighted MR imaging. Radiology. 2005b; 235:190–196. [PubMed: 15703311]

Leone DP, Relvas JB, Campos LS, Hemmi S, Brakebusch C, Fässler R, ffrench-Constant C, Suter U. Regulation of neural progenitor proliferation and survival by β1 integrins. Journal of Cell Science. 2005; 118:2589–2599. [PubMed: 15928047]

Levison SW, Chuang C, Abramson BJ, Goldman JE. The migrational patterns and developmental fates of glial precursors in the rat subventricular zone are temporally regulated. Development. 1993; 119:611–622. [PubMed: 8187632]

Levison SW, Young GM, Goldman JE. Cycling cells in the adult rat neocortex preferentially generate oligodendroglia. Journal of Neuroscience Research. 1999; 57:435–446. [PubMed: 10440893]

Lewis PD, Lai M. Cell generation in the subependymal layer of the rat brain during the early postnatal period. Brain Research. 1974; 76:520–525. [PubMed: 4850922]

Libby RT, Champliaud MF, Claudepierre T, Xu Y, Gibbons EP, Koch M, Burgeson RE, Hunter DD, Brunken WJ. Laminin expression in adult and developing retinae: evidence of two novel CNS laminins. The Journal of Neuroscience. 2000; 20:6517–6528. [PubMed: 10964957]

Liesi P. Do neurons in the vertebrate CNS migrate on laminin? The EMBO Journal. 1985; 4:1163–1170. [PubMed: 4006911]

Loulier K, Lathia JD, Marthiens V, Relucio J, Mughal MR, Tang S-C, Coksaygan T, Hall PE, Chigurupati S, Patton B, Colognato H, Rao MS, Mattson MP, Haydar TF, ffrench-Constant C. β1 integrin maintains integrity of the embryonic neocortical stem cell niche. PLoS Biol. 2009; 7:e1000176. [PubMed: 19688041]

Machold R, Hayashi S, Rutlin M, Muzumdar MD, Nery S, Corbin JG, Gritli-Linde A, Dellovade T, Porter JA, Rubin LL, Dudek H, McMahon AP, Fishell G. Sonic hedgehog is required for progenitor cell maintenance in telencephalic stem cell niches. Neuron. 2003; 39:937–950. [PubMed: 12971894]

Machon O, van den Bout CJ, Backman M, Kemler R, Krauss S. Role of β-catenin in the developing cortical and hippocampal neuroepithelium. Neuroscience. 2003; 122:129–143. [PubMed: 14596855]

Marshall CAG, Novitch BG, Goldman JE. Olig2 directs astrocyte and oligodendrocyte formation in postnatal subventricular zone cells. The Journal of Neuroscience. 2005; 25:7289–7298. [PubMed: 16093378]

Marshall CAG, Suzuki SO, Goldman JE. Gliogenic and neurogenic progenitors of the subventricular zone: Who are they, where did they come from, and where are they going? Glia. 2003; 43:52–61. [PubMed: 12761867]

Mirzadeh Z, Merkle FT, Soriano-Navarro M, Garcia-Verdugo JM, Alvarez-Buylla A. Neural stem cells confer unique pinwheel architecture to the ventricular surface in neurogenic regions of the adult brain. Cell Stem Cell. 2008; 3:265–278. [PubMed: 18786414]

Miyagoe-Suzuki Y, Nakagawa M, Takeda S. Merosin and congenital muscular dystrophy. Microscopy Research and Technique. 2000; 48:181. [PubMed: 10679965]

Miyagoe Y, Hanaoka K, Nonaka I, Hayasaka M, Nabeshima Y, Arahata K, Nabeshima Y-i, Takeda Si. Laminin alpha2 chain-null mutant mice by targeted disruption of the Lama2 gene: a new model of merosin (laminin 2)-deficient congenital muscular dystrophy. FEBS Letters. 1997; 415:33–39. [PubMed: 9326364]

Miyata T, Kawaguchi A, Saito K, Kawano M, Muto T, Ogawa M. Asymmetric production of surface-dividing and non-surface-dividing cortical progenitor cells. Development. 2004; 131:3133–3145. [PubMed: 15175243]

Nishiyama A. Polydendrocytes: NG2 cells with many roles in development and repair of the CNS. The Neuroscientist. 2007; 13:62–76. [PubMed: 17229976]

Nishiyama A, Komitova M, Suzuki R, Zhu X. Polydendrocytes (NG2 cells): multifunctional cells with lineage plasticity. Nature Reviews Neuroscience. 2009; 10:9–22. [PubMed: 19096367]

Noctor SC, Martinez-Cerdeno V, Ivic L, Kriegstein AR. Cortical neurons arise in symmetric and asymmetric division zones and migrate through specific phases. Nature Neuroscience. 2004; 7:136–144. [PubMed: 14703572]

Philpot J, Cowan F, Pennock J, Sewry C, Dubowitz V, Bydder G, Muntoni F. Merosin-deficient congenital muscular dystrophy: the spectrum of brain involvement on magnetic resonance imaging. Neuromuscular Disorders. 1999; 9:81–85. [PubMed: 10220862]

Rakic P. Elusive radial glial cells: Historical and evolutionary perspective. Glia. 2003; 43:19–32. [PubMed: 12761862]

Relucio J I, Tzvetanova D, Ao W, Lindquist S, Colognato H. Laminin alters fyn regulatory mechanisms and promotes oligodendrocyte development. The Journal of Neuroscience. 2009; 29:11794–11806. [PubMed: 19776266]

Romanko MJ, Rothstein RP, Levison SW. Neural stem cells in the subventricular zone are resilient to hypoxia/ischemia whereas progenitors are vulnerable. Journal of Cerebral Blood Flow & Metabolism. 2004; 24:814–825. [PubMed: 15241190]

Roth KA, Kuan C-Y, Haydar TF, D'Sa-Eipper C, Shindler KS, Zheng TS, Kuida K, Flavell RA, Rakic P. Epistatic and independent functions of caspase-3 and Bcl-XL in developmental programmed cell death. Proceedings of the National Academy of Sciences. 2000; 97:466–471.

Rothstein RP, Levison SW. Gray matter oligodendrocyte progenitors and neurons die caspase-3 mediated deaths subsequent to mild perinatal hypoxic/ischemic insults. Developmental Neuroscience. 2005; 27:149–159. [PubMed: 16046849]

Sessa A, Mao C-a, Hadjantonakis A-K, Klein WH, Broccoli V. Tbr2 directs conversion of radial glia into basal precursors and guides neuronal amplification by indirect neurogenesis in the developing neocortex. Neuron. 2008; 60:56–69. [PubMed: 18940588]

Shen Q, Wang Y, Kokovay E, Lin G, Chuang SM, Goderie SK, Roysam B, Temple S. Adult SVZ stem cells lie in a vascular niche: a quantitative analysis of niche cell-cell interactions. Cell Stem Cell. 2008; 3:289–300. [PubMed: 18786416]

Sunada Y, Bernier SM, Kozak CA, Yamada Y, Campbell KP. Deficiency of merosin in dystrophic dy mice and genetic linkage of laminin M chain gene to dy locus. Journal of Biological Chemistry. 1994; 269:13729–13732. [PubMed: 8188645]

Sunada Y, Edgar T, Lotz B, Rust R, Campbell K. Merosin-negative congenital muscular dystrophy associated with extensive brain abnormalities. Neurology. 1995; 45:2084–2089. [PubMed: 7501163]

Tavazoie M, Van der Veken L, Silva-Vargas V, Louissaint M, Colonna L, Zaidi B, Garcia-Verdugo JM, Doetsch F. A specialized vascular niche for adult neural stem cells. Cell Stem Cell. 2008; 3:279–288. [PubMed: 18786415]

Villanova M, Sewry C, Malandrini A, Toti P, Muntoni F, Merlini L, Torelli S, Tosi P, Maraldi N, Guazzi G. Immunolocalization of several laminin chains in the normal human central and peripheral nervous system. Journal of Submicroscopic Cytology and Pathology. 1997; 29:409–413. [PubMed: 9267051]

Walsh C, Cepko C. Clonally related cortical cells show several migration patterns. Science. 1988; 241:1342–1345. [PubMed: 3137660]

Yu Y, Gu S, Huang H, Wen T. Combination of bFGF, heparin and laminin induce the generation of dopaminergic neurons from rat neural stem cells both in vitro and in vivo. Journal of the Neurological Sciences. 2007; 255:81–86. [PubMed: 17360004]

Zerlin M, Levison S, Goldman J. Early patterns of migration, morphogenesis, and intermediate filament expression of subventricular zone cells in the postnatal rat forebrain. The Journal of Neuroscience. 1995; 15:7238–7249. [PubMed: 7472478]

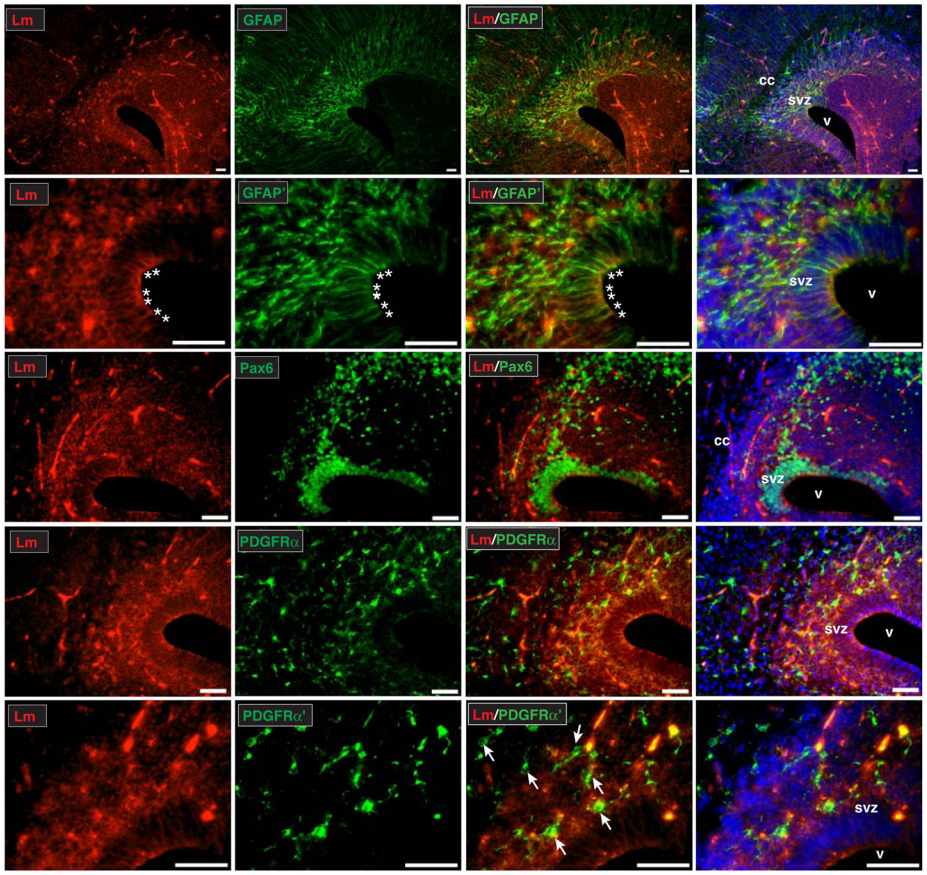

Figure 1. Stem and progenitor cells of the SVZ are found in contact with laminin at the onset of postnatal gliogenesis

Immunohistochemistry with a laminin γ1 subunit (Lm, red) antibody on 25μm coronal sections of cerebral cortices reveals high levels of laminin expression in the SVZ and adjacent regions at postnatal day 1. Laminin immunohistochemistry was performed in conjunction with the following cell lineage specific antibodies: GFAP (green, to visualize radial glia and stem/progenitors of the SVZ), Pax6 (green, to visualize stem/progenitor nuclei in the SVZ and adjacent regions), and PDGFRα (green, to visualize OPCs). In the case of higher magnification images (Lm/GFAP′ and Lm/PDGFRα′), images shown are maximal projections of z-stacks of either 10.7 μm (Lm/GFAP′) or 12.4 μm (Lm/PDGFRα′). Pericellular laminin immunoreactivity was observed in the SVZ and adjacent regions, as well as in blood vessel basal lamina. Prominent laminin immunoreactivity was additionally seen in conjunction with apical radial glial endfeet (Lm/GFAP′ panel, endfeet indicated with asterisks), as well as along radial glial processes themselves. Examples of PDGFRα+ cells in the SVZ (often in contact with laminin) are indicated (Lm/PDGFRα′ panel, arrows). Nuclei are visualized using DAPI (blue). Scale bar in all images is equal to 50 microns. cc, corpus callosum; svz, subventricular zone; v, lateral ventricle.

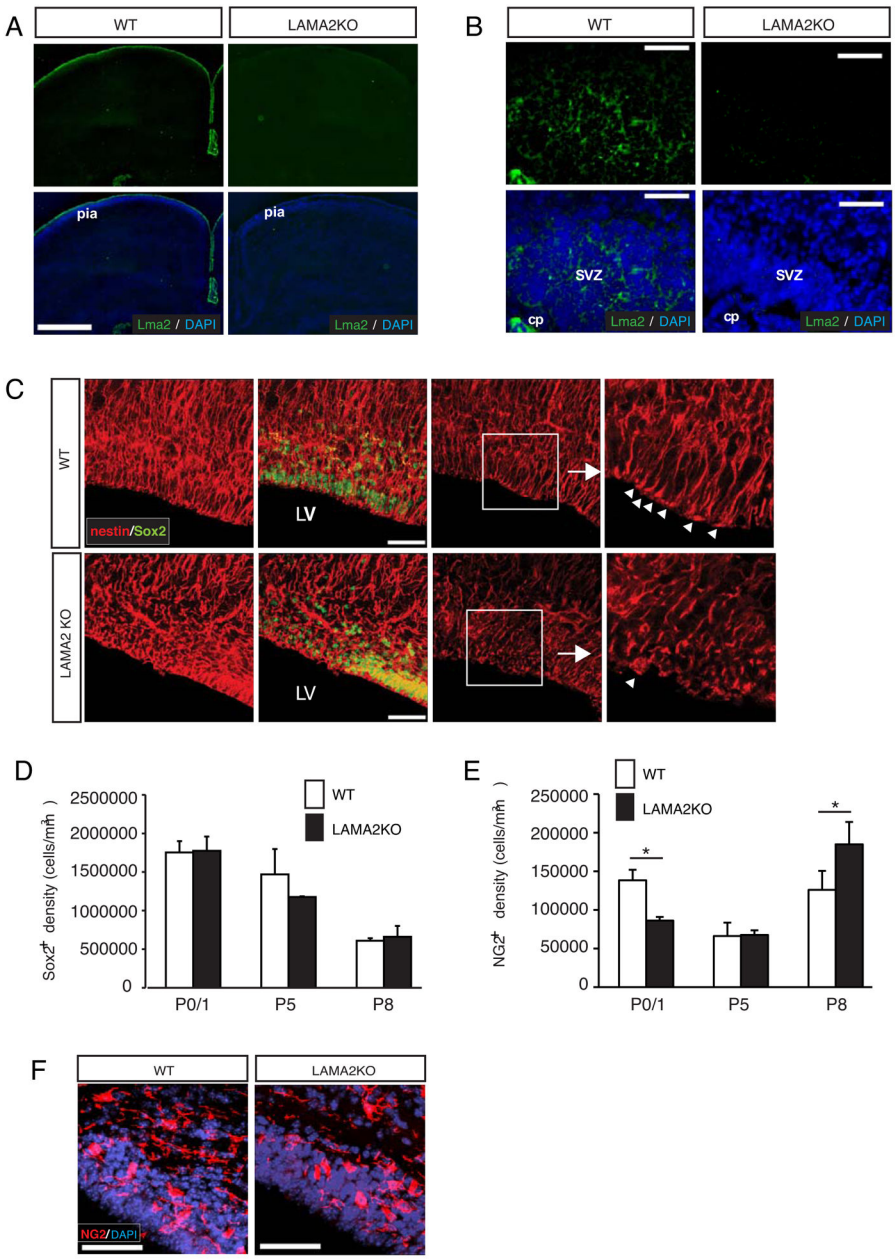

Figure 2. Abnormal progenitor cell organization and density in the postnatal SVZ of laminin α2-knockout mice

(A) Laminin α2 (Lma2) immunoreactivity (green) was observed in the pial basal lamina surrounding wildtype (WT) cortices, but was absent in laminin α2-knockout (LAMA2KO) cortices. Scale bar=500 microns. **(B)** Laminin α2 protein (Lma2; green) was detected in the subventricular zone (SVZ) and choroid plexus (cp) of wildtype mice (WT) at P1, but not in laminin mutant (LAMA2KO) SVZ. Scale bar=50 microns. **(C)** Using immunohistochemistry on floating 40 micron sections, radial glial cells (nestin$^+$, red) and neural stem/intermediate progenitor cell nuclei (Sox2$^+$, green) were visualized using projected images in the SVZ of LAMA2KO mice or wildtype (WT) littermates at P0. Radial glial cells appeared disorganized at the apical surface of the lateral ventricle (LV) in

LAMA2KO mice (inset, right). Scale bar=50 microns. Right panels: nestin (red) and Sox2 (green) immunocytochemistry in representative single plane images of wildtype (WT) and mutant (LAMA2KO) SVZ obtained at higher magnification. Scale bar=20 microns. Small arrows indicate radial glial endfeet at their sites of apical attachment. **(D)** $Sox2^+$ progenitor cells per mm^3 in the SVZ in wildtype (white bars, WT) and mutant (black bars, LAMA2KO) littermates at ages postnatal day 0/1 (P0/1), P5, and P8. Graphs are mean (±sem) counts obtained from 3 different areas of the dorsal SVZ (n=3). **(E)** Oligodendrocyte progenitor cells (NG2+) per mm^3 in the dorsal SVZ in wildtype (white bars, WT) and laminin α2-knockout (black bars, LAMA2KO) littermates at ages P0/1, P5, and P8. Graphs are mean (±sem) counts obtained from 3 different areas of the dorsal SVZ (n=4; *p<0.05). **(F)** Representative images of NG2 (red) immunocytochemistry in the postnatal SVZ of wildtype (WT) and mutant (LAMA2KO) mice. Compared to wildtype (WT), LAMA2KO mice have fewer $NG2^+$ cells in the SVZ at P1. Scale bar=50 microns. Nuclei are visualized using DAPI (blue).

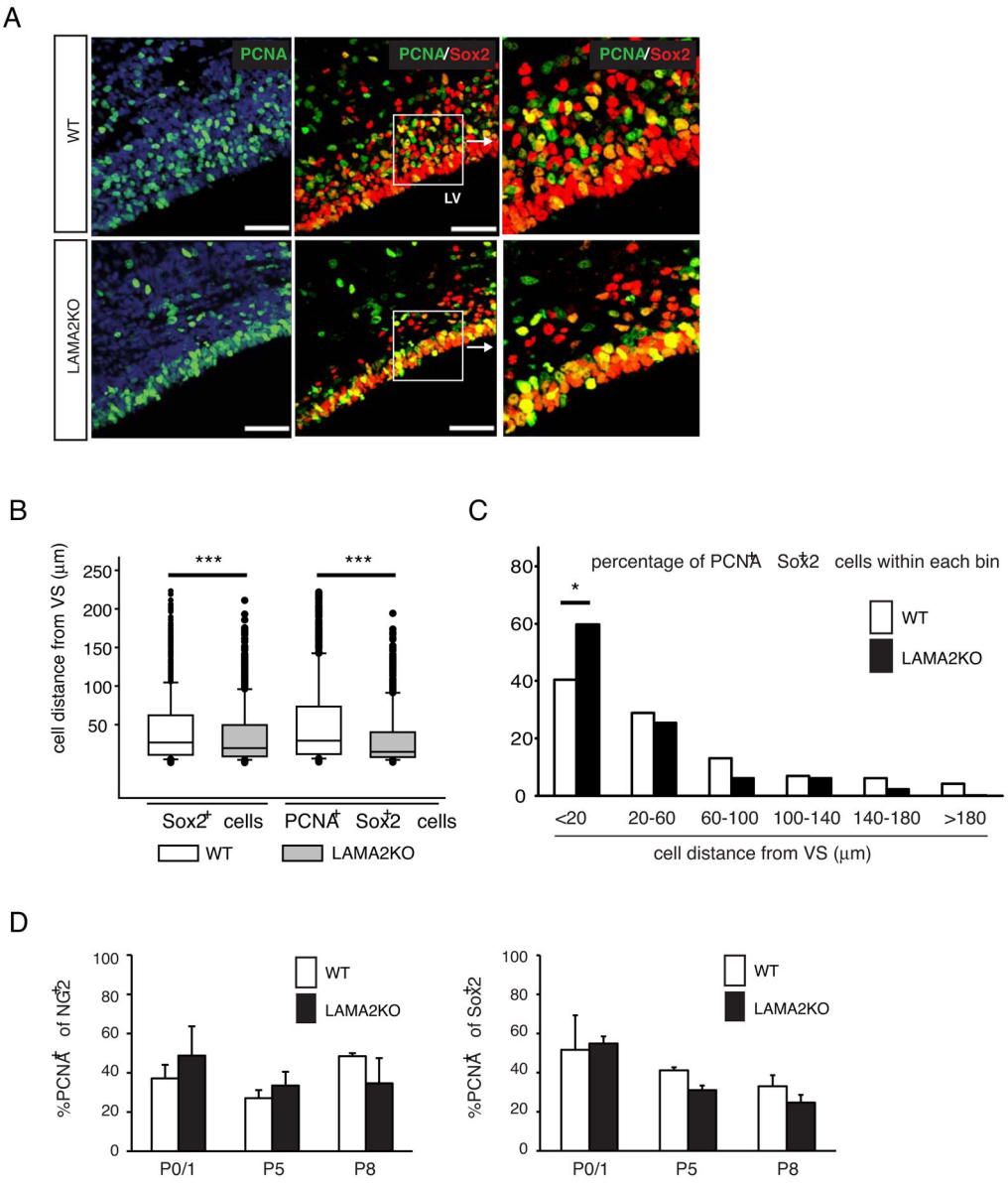

Figure 3. Altered positioning of proliferative Sox2$^+$ progenitor cells in the laminin α2 knockout SVZ

(A) *Leftmost panels*: representative images of PCNA (green) immunocytochemistry in wildtype (WT) and mutant (LAMA2KO) SVZ. *Middle panels*: representative images of Sox2 (red) and PCNA (green) immunocytochemistry in wildtype (WT) and mutant (LAMA2KO) SVZ. Scale bars=50 microns. Proliferating Sox2$^+$ cells were found abnormally close to the lateral ventricle (LV) in the LAMA2KO SVZ (inset, right), compared to that seen in the WT SVZ (inset, right). Nuclei were visualized using DAPI (blue). **(B)** Box plots of the distances of Sox2$^+$ and proliferating i.e. PCNA$^+$, Sox2$^+$ cells from the ventricle surface (VS) in wildtype (white boxes; WT) and mutant (gray boxes; LAMA2KO) dorsal SVZ at P1. Each horizontal line represents the 10th, 25th, 50th (median), 75th and 90th percentiles. Based on median distance values (center bar), Sox2$^+$ and PCNA$^+$Sox2$^+$ cells can be found significantly closer to the VS in the LAMA2KO SVZ

compared to WT (n=1065–1378 total $Sox2^+$ cells; n=564–788 $PCNA^+$ cells within the $Sox2^+$ population; ***$p<0.001$). **(C)** Individual $PCNA^+Sox2^+$ cell distance measurements were grouped to reveal that an increased percentage of proliferating $Sox2^+$ cells were positioned closer (i.e., <20 microns away) to the ventricular surface (VS) in the SVZ of laminin α2-knockout mice (black bars; LAMA2KO), compared to the wildtype (white bars; WT) SVZ (*$p<0.05$). **(D)** *Left panel*: Percentages of PCNA-positive cells within the $NG2^+$ cell population of the SVZ were not significantly different between wildtype (white bars; WT) and laminin α2-knockout (black bars; LAMA2KO) mice at postnatal day 0/1 (P0/1), P5, and P8 ($n=3$). *Right panel*: The percentages of PCNA-positive cells within the $Sox2^+$ cell population were also determined in wildtype (white bars; WT) and laminin α2-knockout (LAMA2KO) SVZ at P0/1, P5, and P8 ($n=3$). No significant differences were observed between WT and LAMA2KO animals at these timepoints. Graphed values depict mean (±sem) percentages obtained from 3 different regions of the dorsal SVZ.

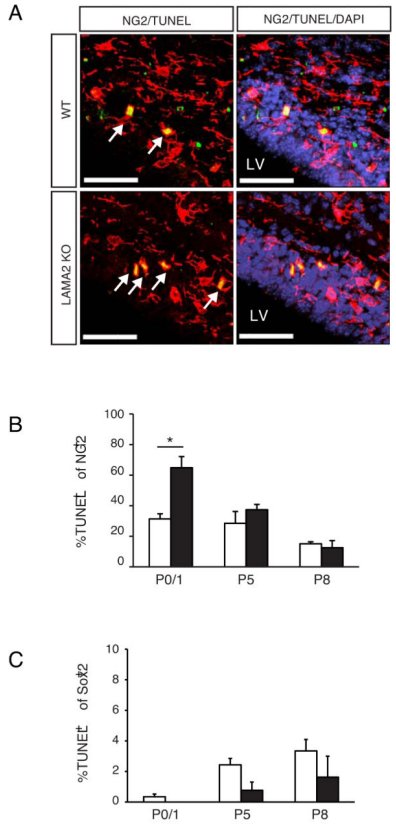

Figure 4. Elevated levels of oligodendrocyte progenitor death in the LAMA2KO subventricular zone

(A) NG2 immunocytochemistry (red) to visualize oligodendrocyte progenitor cells was performed in combination with TUNEL to detect dying cells (green). Representative fields are shown from P1 wildtype (WT) and laminin α2-knockout (LAMA2KO) SVZ dorsal to the lateral ventricle (LV). Arrows depict TUNEL$^+$NG2$^+$ cells. Scale bars=50 microns. **(B)** Percentages of TUNEL$^+$ cells in the NG2$^+$ populations in the dorsal SVZ were determined in wildtype (white bars, WT) and laminin α2-knockout (black bars, LAMA2KO) littermates at ages P0/1, P5, and P8. A significant increase in OPC death was observed in the SVZ of mutant mice compared to wildtype. Graphs are mean (±sem) counts obtained from 3 different areas of the dorsal SVZ (n=3; *p<0.05). **(C)** No significant differences in Sox2$^+$ cell-specific apoptosis were observed between wildtype and laminin α2 knockout mice. Percentages of TUNEL-positive cells in the Sox2$^+$ populations in the SVZ were determined in wildtype (white bars, WT) and laminin α2-knockout (black bars, LAMA2KO) littermates at ages P0/1, P5, and P8. Graphs are mean (±sem) counts obtained from 3 fields in the dorsal SVZ (n=3).

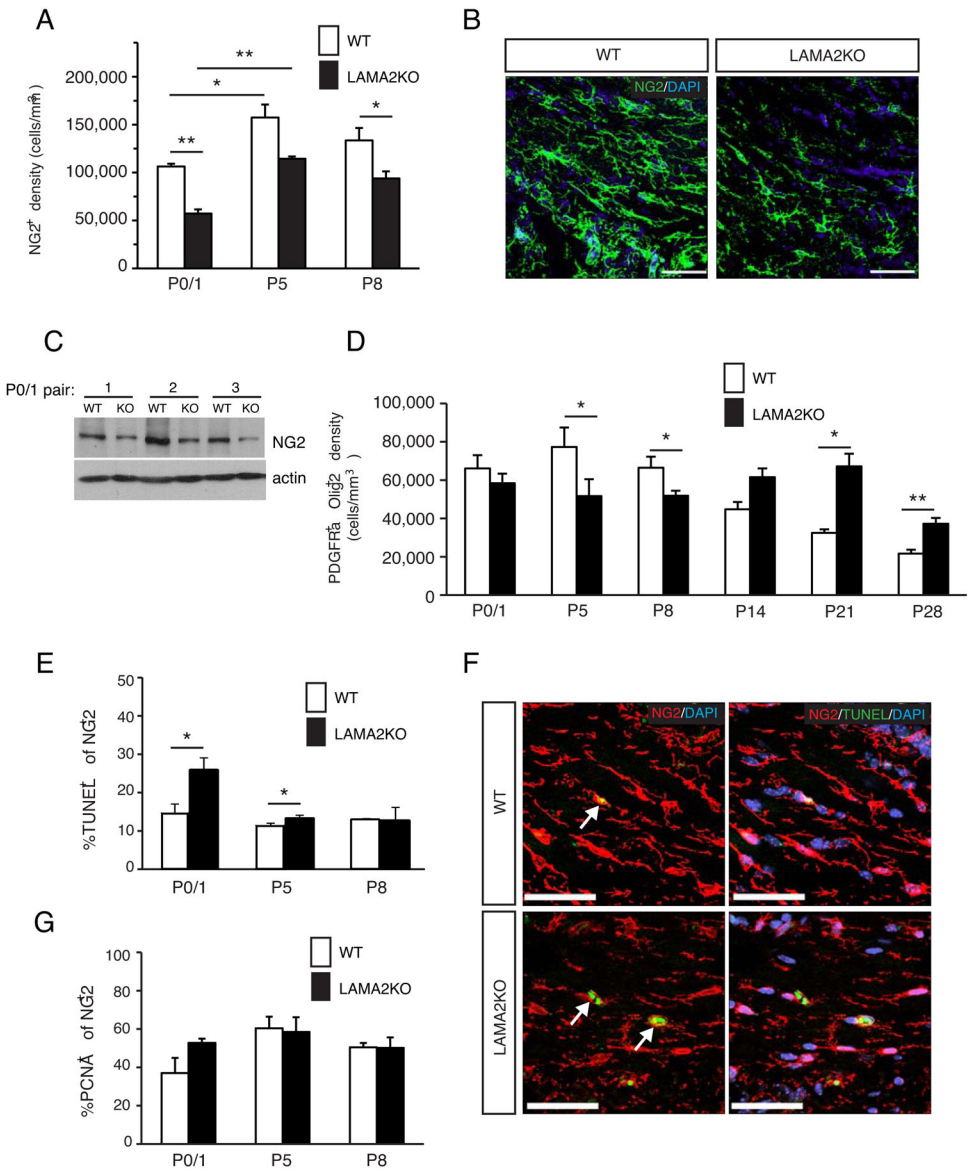

Figure 5. Oligodendrocyte progenitor cell densities are abnormal in the developing white matter of LAMA2KO mice

(A) Mean density of NG2-positive oligodendrocyte progenitor cells (OPCs) per white matter volume (mm^3) is shown for wildtype (white bars; WT) and laminin α2-knockout (black bars; LAMA2KO) corpus callosum at P0/1, P5, and P8. Loss of laminin α2 leads to significant decreases in the density of $NG2^+$ OPCs in the corpus callosum during early postnatal development. Graphs are mean (±sem) counts obtained from 4 different areas of the corpus callosum (*p<0.05, **p<0.01, n=3–4). **(B)** Representative fields from P1 wildtype (WT) and laminin α2-knockout (LAMA2KO) corpus callosum are shown. NG2 immunocytochemistry (green) was performed to visualize OPCs. Nuclei were stained with DAPI (blue). Scale bars denote 50 microns. **(C)** Cerebral cortical lysates were evaluated by Western blot to detect protein levels of NG2 or actin (loading control). Representative blots from P0/1 wildtype (WT) and laminin α2-knockout (KO) littermates show decreased NG2

protein levels in KO cortical lysates relative to those from WT littermates (n=3). **(D)** Mean densities of cells that were double positive for PDGFRα (a marker expressed in OPCs, but not in differentiated oligodendrocytes) and Olig2 (a transcription factor expressed in oligodendrocyte lineage cells) per volume (mm^3) of the WT (white bars) and LAMA2KO (black bars) corpus callosum were evaluated at 6 developmental timepoints (i.e., P0/1, P5, P8, P14, P21, and P28). Prior to P14, LAMA2KO mice had significantly less $PDGFR\alpha^+Olig2^+$ cells in the corpus callosum than their WT littermates. After the 2-week timepoint, however, the numbers of $PDGFR\alpha^+Olig2^+$ OPCs were significantly higher in the LAMA2KO corpus callosum than in WT. Graphed values are mean (±sem) cell densities measured from 4 different areas of the corpus callosum ($*p<0.05$, $**p<0.01$, n=3). **(E)** Graph depicts mean percentages of TUNEL-positive cells out of the $NG2^+$ OPC population in the wildtype (white bars; WT) and laminin α2-knockout (black bars; LAMA2KO) corpus callosum, at 3 different postnatal timepoints (n=3–5). Increased OPC apoptosis (i.e., $\%TUNEL^+$ of $NG2^+$ cells) was observed in the LAMA2KO corpus callosum at early postnatal timepoints (i.e., P1 and P5; $*p<0.05$). **(F)** Representative images taken from P1 wildtype (WT) and laminin α2-knockout (LAMA2KO) corpus callosum are shown. NG2 immunocytochemistry (Kerever et al.) was performed in combination with TUNEL (green) to detect apoptotic OPCs in the developing white matter tracts of WT and LAMA2KO mice at P1. Arrows depict TUNEL-positive $NG2^+$ cells. Nuclei were counterstained with DAPI (blue). Scale bars denote 50 microns. **(G)** The percentages of proliferating OPCs were determined in the wildtype (white bars; WT) and laminin α2-knockout (black bars; LAMA2KO) at P0/1, P5, and P8 by immunohistochemistry with antibodies against PCNA (a marker of proliferating cells) and NG2. In the corpus callosum, no significant differences were observed in the mean percentages of PCNA-positive cells in the $NG2^+$ OPCs of WT and LAMA2KO mice (n=3).

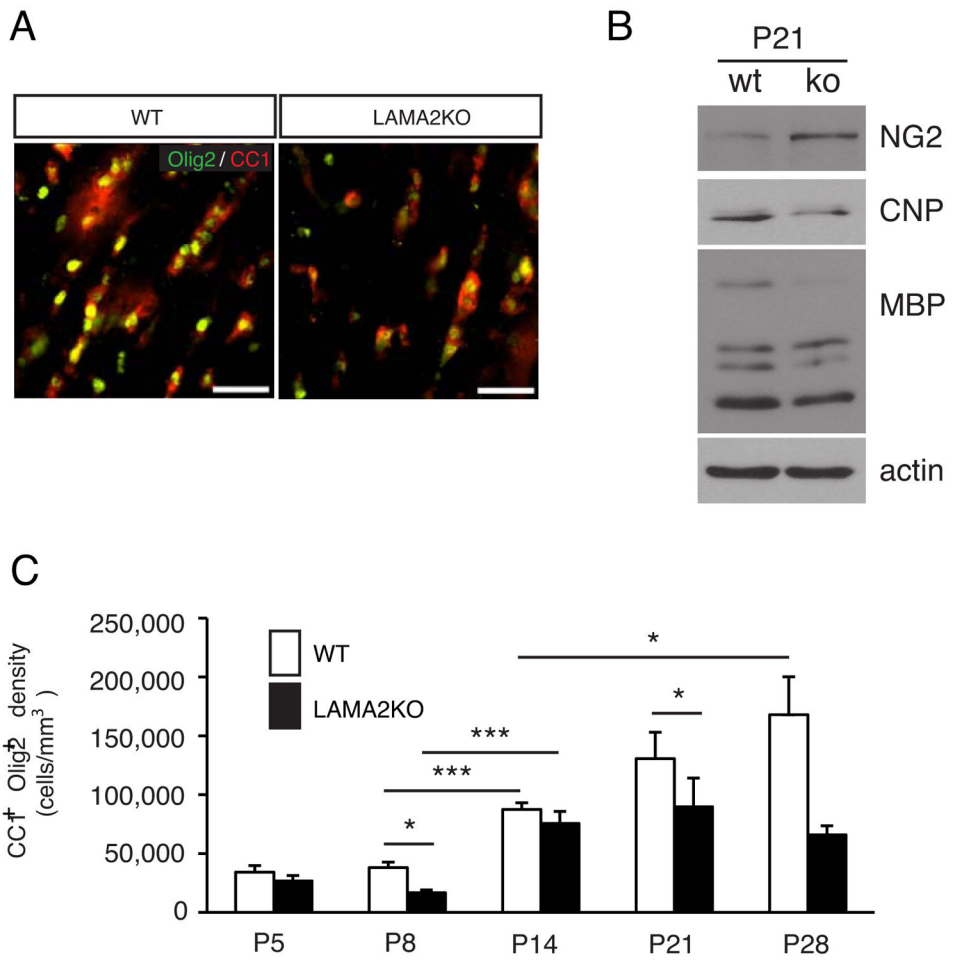

Figure 6. Defective oligodendrocyte maturation in laminin α2-knockout brains

(A) Immunocytochemistry using anti-CC1 (a marker of mature oligodendrocytes, red) and anti-Olig2 (a pan-oligodendrocyte lineage cell marker, green) antibodies was performed to visualize mature oligodendrocyte cells. Representative fields are shown from P21 wildtype (WT) and laminin α2-knockout (LAMA2KO) corpus callosum. Scale bar=50 microns. **(B)** Representative western blots of cerebral cortical lysates from P21 wildtype (WT) and laminin α2-knockout (LAMA2KO) littermates show differential expression of oligodendrocyte stage specific protein markers. Compared to wildtype mice, LAMA2KO animals had elevated levels of the NG2 protein (expressed in oligodendrocyte progenitors) and decreased levels of the oligodendrocyte maturation markers CNP and MBP. Actin was used as a loading control. **(C)** The mean cell densities co-expressing CC1 and Olig2 per volume (mm^3) of corpus callosum were determined for wildtype (white bars, WT) and laminin α2-knockout (black bars, LAMA2KO) animals at 5 postnatal timepoints (i.e., P5, P8, P14, P21, and P28). LAMA2KO mice had significantly fewer $CC1^+Olig2^+$ mature oligodendrocytes in the white matter compared to their WT littermates at various timepoints analyzed. (n=3–4, $*p<0.05$, $***p<0.005$). Graphs depict mean (±sem) cell densities measured from 4 different areas of the corpus callosum.

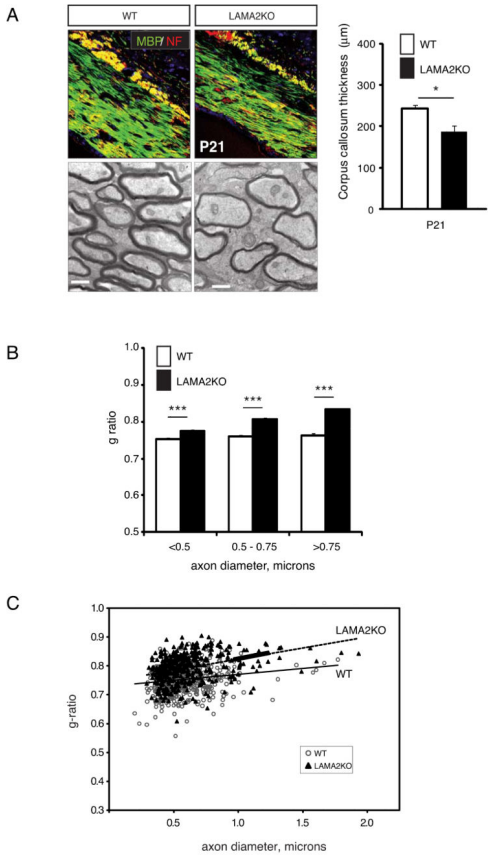

Figure 7. Abnormal myelin in the laminin α2-knockout corpus callosum

(A) *Top panels:* immunocytochemistry to visualize MBP (green) and neurofilament (Blaess et al.; Kerever et al.) in wildype (WT) and laminin α2-knockout (LAMA2KO) 3 week-old corpus callosum. Sections are counterstained with DAPI (blue) to visualize nuclei. Scale bars=50 microns. *Bottom panels*: Representative electron micrographs of the corpus callosum revealed thinner myelin in the axons of the LAMA2KO corpus callosum relative to WT at P21. Scale bars=500nm. **(B)** The mean thickness of the corpus callosum was measured in wildtype (white bars, WT) and laminin α2-knockout (black bars, LAMA2KO) animals at P21. LAMA2KO mice had significantly thinner corpora callosa compared to their WT littermates at P21 (n=4, *p<0.05). Graph depicts mean (±sem) callosal thickness values. **(C)** Axon g-ratios were binned by axon diameter to reveal that axons of all sizes in LAMA2KO corpus callosum (black bars) had thinner myelin (i.e., higher median g-ratios) compared to wildtype (white bars) (***p<0.001). **(D)** Corpora callosa g-ratios were plotted as a function of axon diameter for wildtype (open circles; WT) and laminin α2-knockout (black triangles; LAMA2KO) P21 mice. Overall median g-ratios were significantly different (p<0.001) between WT and LAMA2KO axons in the corpus callosum (0.822; n=567 axons evaluated in 3 laminin α2-knockout animals compared to 0.755; n=387 axons analysed in 2 wildtype littermates). No change was observed in the corpus callosum as to the degree of unmyelinated axons.

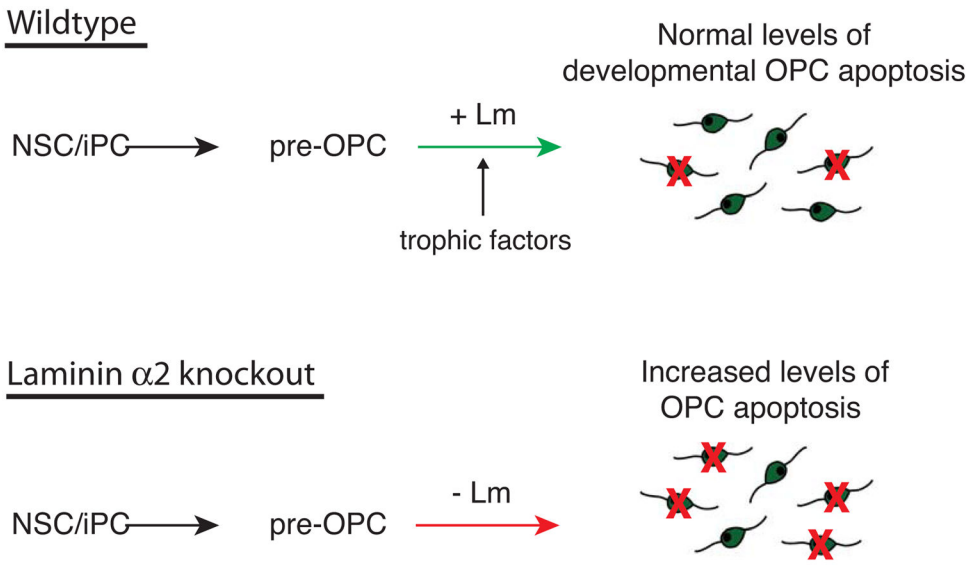

Figure 8. Laminin in the SVZ helps to ensure appropriate numbers of OPCs

Many newly-born oligodendrocyte progenitor cells (OPCs) die due to developmental programmed cell death in the perinatal SVZ. However, OPC death is significantly elevated in the subventricular zone (SVZ) and adjacent white matter tract of early postnatal laminin-knockout brains. Laminin thus promotes the survival of OPCs in the gliogenic niche, allowing the appropriate numbers of OPCs to populate their target white matter tracts. This survival-promoting effect is likely indirect e.g. by localizing or enhancing trophic factor signals, as isolated OPCs do not survive better on laminin substrates.